TITLE PAGE

Age-associated failure of efficient cardiac proteostatic adaptations to chronic cAMP-stress is associated with accelerated heart aging

*Maria Grazia Perino PhD[1], *Miguel Calvo-Rubio Barrera PhD[2], Giulio Agnetti PhD[3], Mark Ranek PhD[3], Daniel R. Riordon BS[1], Christopher H. Morrell PhD[1], Khalid Chakir PhD[1], Jia-Hua Qu PhD[4], Kirill V Tarasov PhD[1], Admira Parveen BS[3], Hikmet Kadioglu MD[3], Rafael De Cabo PhD[2], Edward G. Lakatta MD[1]

*Contributed equally

Correspondence to: Maria Grazia Perino, PhD, Laboratory of Cardiovascular Science, National Institute on Aging, National Institutes of Health, 251 Bayview Blvd, Baltimore (MD) 21224, United States, Email: mariagrazia.perino@nih.gov

Affiliations:

[1]Laboratory of Cardiovascular Science, National Institute on Aging, National Institutes of Health, Baltimore, United States

[2]Translational Gerontology Branch, Intramural Research Program, National Institute on Aging, National Institutes of Health, Baltimore, United States

[3]Division of Cardiology, Department of Medicine, Johns Hopkins University School of Medicine, Baltimore, United States

[4]University of California, San Francisco

Total word count: ~10200

ABSTRACT

BACKGROUND: Dysregulated proteostasis leading to accumulation of misfolded proteins, electron-dense aggregates (lipofuscin, LF), desmin preamyloid oligomers (PAOs), and proteotoxic stress is a hallmark of aging. We investigated how efficiently proteostatic adaptations to chronic cardiac cyclic adenosine monophosphate (cAMP)-dependent stress change with aging, in mice harboring a marked, cardiac-specific over-expression of adenylyl cyclase VIII (TG^{AC8}).

METHODS: Protein quality control (PQC) mechanisms (ubiquitin proteasome system (UPS) and autophagy), including mitophagy, in TG^{AC8} and wild time littermates (WT) were evaluated in left ventricle (LV) at 3-4 months and at 17-21 months of age. Autophagy flux was evaluated in response to the lysosomotropic agent chloroquine (CQ), and protein synthesis was assessed according to the SUnSET puromycin method.

RESULTS: At 3-4 months of age, established autophagy markers such as the microtubule-associated protein 1 light chain 3 (LC3), p62, and their phospho-forms in TG^{AC8} LV were modulated to result in a more efficient autophagy. Flux was increased compared to WT. Lysosome performance (cathepsin L1 activity) in TG^{AC8} was also significantly increased, confirming higher cargo degradation and a more efficient proteostasis at 3-4 months. In advanced age, however, insufficiency of PQC mechanisms, manifested by a reduced proteasome activity, and an unbalanced autophagic flux, accelerated for markers such as LC3A and p62 within the context of a slower *overall* flux, led to an increase in the accumulation of aggresomes (increased ratio

of insoluble/soluble protein fractions). In addition, although at 3-4 months canonical mitophagy signaling was increased (receptors PARKIN, p62-S403 and p62-S349 were upregulated) and non-canonical mitophagy signaling not engaged (receptor FKBP8 was decreased), both were upregulated at 18-21 months of age in TG^{AC8}, as protein levels of all receptors remained elevated. In old TG^{AC8}, the markedly impaired mitophagy, accompanied by the accumulation of lipofuscin (LF) bodies of aberrant sizes and brownish-to black pigment, increased concentration of cardiac preamyloid oligomers (PAOs) and elevated levels of cleaved desmin, tagged for ubiquitination, were characteristics of the age-effect compared to young TG^{AC8}. The rate of protein synthesis and levels of soluble aggregates were decreased, consequences of “normal” aging.

CONCLUSIONS: Proteostasis maintains cardiac health in TG^{AC8} in youth (3-4 months), but a long-term exposure to chronic pathophysiologic states that increase cardiac ubiquitination and stress, in response to sustained activation of the AC/cAMP/PKA/Ca^{2+} axis, results in severely dysregulated proteostasis in TG^{AC8} vs WT, and is associated with proteostatic insufficiency, and accelerated cardiac aging.

GRAPHIC ABSTRACT: A graphic abstract is available for this article.

Key Words: proteostasis, cardiac stress, chloroquine, mitophagy, aging

Nonstandard Abbreviations and Acronyms

LF lipofuscin

PAOs preamyloid oligomers

70 **cAMP** cyclic adenosine monophosphate

71 **AC** adenylyl cyclase

72 **AC8** adenylyl cyclase VIII

73 **PQC** protein quality control

74 **UPS** ubiquitin proteasome system

75 **CQ** chloroquine

76 **LC3** microtubule-associated protein 1 light chain 3

77 **LV** left ventricle

78 **HF** heart failure

79 **PE** phosphatidylethanolamine

80 **PKA/PKC** protein kinase A/ protein kinase C

81 **KEAP1** Kelch-like ECH-associated protein 1

82 **NRF2** transcription factor NF-E2-related factor 2

83 **ACP2** lysosomal acid phosphatase

84 **ATG4B** autophagy related 4B cysteine peptidase

85 **TEM** transmission electron microscopy

86 **ROS** reactive oxygen species

87

88 # INTRODUCTION

89 Cardiac proteostasis, protein quality control (PQC) in the context of balanced protein
90 synthesis and degradation, is required maintenance for cardiac health. Pathogenic
91 aspects of protein misfolding and aggregation are collectively referred to *proteotoxicity*. A
92 proteotoxic insult that accompanies advanced age can ultimately lead to heart
93 dysfunction[1], and eventual cardiac failure[2]. Many protein aggregate–based diseases in
94 the heart have been well characterized[3]. Plaque deposition (amyloidosis) or accumulation
95 of soluble, oligomeric aggregates, and, more recently, desmin disorganization and the
96 increase in the heart of desmin preamyloid oligomers (PAOs)[4] with aging, have also
97 emerged as common hallmarks of acquired heart failure (HF)[5,6,7].

98 Many factors, including the imbalance in protein synthesis and degradation,
99 exhaustion of the proteostasis machinery, and downregulation of clearing mechanisms,
100 such as the ubiquitin proteasome system (UPS) and autophagy[8], can lead to proteostatic
101 collapse. Impaired autophagy and mitophagy that accompany advancing age due to
102 reduced lysosomal[9] and mitochondrial fitness by increased oxidative stress[10], have been
103 linked to the accumulation of electron-dense aggregates, generally referred to lipofuscin
104 (LF). Accumulation of LF as age advances, occurs as proteostatic mechanisms begin to
105 collapse[11], and repair or breakdown of damaged proteins and organelles become
106 deficient. LF linearly increases during with aging, and is inversely correlated with
107 longevity[12,13]

108 Our recent study demonstrated that chronic severe cardiac stress in response to over-
109 expression of adenylyl cyclase VIII (AC8) in mice (TG^{AC8}), induced concentric adaptation
110 circuitry at young age (3-4 months). This adaptive circuitry includes impressive

111 upregulation of protein synthesis and degradation mechanisms (proteasome and
112 autophagy) that protect against cardiac stress[14], maintaining a remarkable, high
113 performance cardiac phenotype for up to about one year of age[15-18]. But, signs of chronic
114 heart failure (CHF) and cardiomyopathy in TG^{AC8} emerge as age advances[18-20]. Here we
115 test the hypothesis that in advanced age the adaptive proteostatic mechanisms in
116 response to severe sustained cAMP-dependent chronic cardiac stress become *more*
117 *impaired* in TG^{AC8} than in WT.

118 # METHODS

119 **Experimental animals**

120 All studies were performed in accordance with the Guide for the Care and Use of
121 Laboratory Animals published by the National Institutes of Health (NIH Publication no. 85-
122 23, revised 1996). All experimental protocols were approved by the Animal Care and Use
123 Committee of the National Institutes of Health (protocol #441-LCS-2019). Breeder pairs
124 of mice in which human TG^{AC8} was over-expressed under the murine α-myosin heavy
125 chain (α-MHC) promoter (TG^{AC8}), and wild-type littermates (WT) (background strain
126 C57BL/6 from Jackson Labs, Stock # 000664), were a gift from Nicole Defer/Jacques
127 Hanoune, Unite de Recherches, INSERM U- 99, Hôpital Henri Mondor, F-94010 Créteil,
128 France[15].

129 Mice were bred and housed in a climate-controlled room with 12-hour light cycle and
130 free access to food and water, as previously described[21]. All assays were performed in
131 3-4-month-old (young) and 17-21-month-old (old) males and compared to age-matched
132 wild-type littermates (WT). Mice were sacrificed using Ketamine/Xylazine mixture, by

133 intraperitoneal (IP) administration, in accordance with the approved protocol (#441-LCS-
134 2019).

135 **Heart and cardiac tissue isolation**

136 The heart was quickly removed and placed into cold PBS solution. The left ventricle
137 (LV) free wall, without the septum, was identified anatomically under a dissecting
138 microscope, excised, snap-frozen in liquid nitrogen and stored at -80°C for further
139 analyses.

140 **Protein extraction and WB**

141 Flash frozen tissue was homogenized as previously described[14]. Briefly, snap-frozen
142 LVs were homogenized and lysed in ice cold RIPA buffer (Thermo Fisher Scientific: 25
143 mM Tris-HCl (pH 7.6), 150 mM NaCl, 1% NP-40, 1% sodium deoxycholate, 0.1% SDS)
144 supplemented with a Halt protease inhibitor cocktail (Thermo Fisher Scientific), Halt
145 phosphatase inhibitor cocktail (Thermo Fisher Scientific) and 1 mM phenylmethyl sulfonyl
146 fluoride, using a Precellys homogenizer (Bertin Instruments) with a tissue homogenization
147 kit CKMix (Bertin Instruments) at 4°C. Extracts were then centrifuged at 10,000g for 10
148 min at 4°C and the protein concentration of the soluble fraction determined using the
149 Bicinchoninic Acid (BCA) Assay (Thermo Fisher Scientific). Samples were denatured in
150 4X Laemmli sample buffer (BioRad Laboratories) containing 355 mM 2-mercaptoethanol
151 at 95°C for 5 min, or DTT at 70°C for 10 min, and proteins (25µg/lane) were resolved on
152 4-20% Criterion TGX Stain Free gels (Bio-Rad Laboratories) by SDS/PAGE. To induce
153 crosslinking of Stain Free gel trihalo compound with protein tryptophan residues gels were
154 exposed to UV transillumination for 2-3 mins. Proteins were then transferred to low
155 fluorescence polyvinylidene difluoride (LF-PVDF) membranes (BioRad Laboratories),
156 using an electrophoretic transfer cell (Mini Trans-Blot, Bio-Rad). Membrane total protein

157 was visualized using an Amersham Imager 600 (AI600) (GE Healthcare Life Sciences)
158 with UV transillumination to induce and capture a fluorescence signal. Blocked
159 membranes (5% milk/tris-buffered saline with Tween-20, TBST) were incubated with the
160 primary antibodies indicated in the **Major Resource Table**. Primary antibodies were then
161 detected using horseradish peroxidase (HRP) conjugated antibody (Invitrogen) at
162 1:5,000, and bands were visualized using Pierce SuperSignal West Pico Plus ECL
163 substrate kits (Thermo Scientific), the signal captured using an Amersham Imager 600
164 (AI600) (GE Healthcare Life Sciences) and quantified using ImageQuant TL software (GE
165 Healthcare Life Sciences). Band density was normalized to total protein, and TG^{AC8} to
166 average of WT.

167 **Proteosome activity assay**

168 Proteasome activity was measured with Proteasome-Glo™ Chymotrypsin-Like
169 Assay G8621, accordingly to the manufacturer's instructions. Briefly, lysed tissue was
170 diluted with the provided buffer and 50 µg of sample was loaded on a 96 well microplate.
171 The resulting "glow-type" luminescent signal was then quantified utilizing the Spectramax
172 microplate reader (San Jose), with luminescence recorded at 500. Human 20S
173 Proteosome was used as a positive control.

174 **Protein aggregation assay**

175 The isolation of protein aggregates and the assessment of protein aggregation was
176 conducted using the Proteostat kit (Enzo Life Science, ENZ-51023), as previously
177 published[14]. Specifically, 50 µg of proteins were loaded into a 96-well plate for analysis.
178 Fluorescence measurements were obtained with an excitation wavelength of 550 nm and
179 emission wavelength of 600 nm, employing a time interval of 15 minutes between
180 readings, and background readings were subtracted from sample recordings.

181 **Cathepsin L1 activity assay**

182 Cathepsin L1 activity was measured using the fluorimetric kit (Abcam, ab65306)
183 according to the manufacturer's instructions. Briefly, snap-frozen LVs stored at -80°C
184 were thawed on ice, and 10 mg of tissue was resuspended in 50 µl of CL Buffer, then
185 homogenized with a Dounce homogenizer sitting on ice, with 10–15 passes. Samples
186 were centrifuged for 2–5 mins at 4°C at top speed using a cold microcentrifuge to remove
187 any insoluble material, then supernatants were collected and transferred to a clean tube,
188 on ice. Activity was performed at different dilutions to reach Vmax, in the presence of Ac-
189 FR-AFC fluorogenic substrate (200 µM final concentration), at 37°C for 1–2 hours, at an
190 excitation wavelength of 400 nm and an emission wavelength of 505 nm using the
191 Cytation 5 microplate reader (Biotek). Fold-increase in Cathepsin L activity was
192 determined by comparing the relative fluorescence units (RFU) with the level of the
193 uninduced control, after subtraction of the negative control sample. TG^{AC8} values were
194 normalized to average of WT.

195 **Quantification of desmin preamyloid oligomers (PAOs)**

196 Myofilament-enriched, insoluble fractions were prepared as described previously[7].
197 Fractions were separated using precast NuPAGE gels (Thermo Fisher Scientific) with
198 MES buffer, and probed with the desmin antibody (DE-U-10, Sigma, 1:10,000) or the A11
199 antibody (kindly provided by Dr. Charles Glabe at UC Irvine[22], 1:1,500). TG^{AC8} values
200 were normalized to WT.

201 **Transmission Electron Microscopy (TEM)**

202 Samples for transmission electron microscopy was fixed using 2.5% glutaraldehyde
203 in 0.1 M sodium cacodylate buffer, pH 7. Then, they were post-fixed in 1% osmium
204 tetroxide for 1 h at 4°C in the same buffer, dehydrated, and then embedded in Embed

205 812 resin (Electron Microscopy Sciences, Hatfield, PA) through a series of resin resin-
206 propylene oxide gradients to pure resin. Blocks were formed in fresh resin contained in
207 silicon molds, and the resin was polymerized for 48-72 h at 65°C; blocks were then
208 trimmed and sectioned in an EM UC7 ultramicrotome (Leica Microsystems, Buffalo
209 Grove, IL) to obtain both semi-thick (0.5-1 μm width) and ultrathin (40-60 nm width)
210 sections. Semi-thick sections were mounted on glass slides and stained with 1% toluidine
211 blue in a 1% borax aqueous solution for 2 min. Palade-stained (OsO4) and Toluidine blue-
212 stained semi-thick sections were then imaged using a Leica AXIO Imager light
213 microscope with a 63x oil immersion objective, for quality control and Lipofuscin (LF)
214 quantification. Ultrathin sections were stained with uranyl acetate and lead citrate and
215 then imaged on a Talos L120C Transmission Electron Microscope (TEM) with a 4K Ceta
216 CMOS camera, for macroautophagic events quantification.

217 Micrographs at ×2000 ×5000 and ×11000 magnification were obtained from randomly
218 selected cytoplasmic areas of cardiomyocytes, for illustration purposes and quantitative
219 analysis of macroautophagic events population. Two stereological parameters were
220 determined: (a) the numerical profile density Na (number of figures of interest / μm2 of
221 cell fraction), and (b) volume density of figures of interest (Vv; i.e., the volume fraction of
222 cardiomyocyte cytoplasm occupied by figures of interest). Volume density was obtained
223 following a point analysis using a simple square lattice test system[23], with superposition
224 of a virtual grid over the micrographs where the user performs a point-counting method.
225 Autophagosomes were identified as double-membrane vesicles with identifiable cargo
226 and comparable density to the surrounding cytosol. Autolysosomes and residual bodies

227 were denoted as single membrane vesicles containing non-identifiable cargo of higher
228 density than the surrounded cytosol and fragmented organelles.

229 Lipofuscin bodies were identified following Palade staining[24] by the presence of
230 densely packed lipids with a dark brown-black color against cardiomyocyte cytosol, which
231 allowed a straightforward segmentation of the image and posterior quantification of the
232 planimetric and stereological parameters. Point counting and areas of vesicles and
233 cytosol were measured using manual tracking with ImageJ software by a blinded
234 investigator.

235 **Statistics**

236 Data are presented as median ± range or median ± interquartile range. Representative
237 TEM images and western blots were chosen based on the resemblance to the average
238 values. Number of samples per group are indicated in each legend. Statistical analyses
239 were performed in GraphPad Prism 9. ROUT analyses were applied to identify outliers,
240 which were excluded from group comparison analyses. Student *t* test with Welch's
241 correction was used to compare data between 2 groups. Two-way ANOVA followed by
242 Original FDR method of Benjamini and Hochberg was used for multiple comparisons[25].
243 For datasets with matching LC3I and LC3II from the same animal, a multiple measures
244 approach with three-way mixed ANOVA or mixed-effect analysis for repeated measures
245 was taken, followed by Original FDR method of Benjamini and Hochberg.

246 # RESULTS

247 **Autophagy is upregulated in the TG^{AC8} heart at 3-4 months of age**

248 To assess basal autophagy in LVs in young TG^{AC8} and WT, we performed WB of the
249 established autophagy markers LC3 and p62/sequestosome-1, and assessed their

250 activity via measuring their phosphorylation states. Both LC3A and LC3B isoforms, which
251 localize on different autophagosomes[26], were assessed using isoform-specific antibodies.
252 Significant changes in the cytosolic LC3**I** and its lipidated product, LC3**II** (LC3-**PE**), that
253 is recruited to the autophagosomal membrane during autophagy, were evident in TG^{AC8}
254 vs WT. Specifically at this age, LC3**AI** was significantly upregulated, in TG^{AC8} vs WT,
255 whereas LC3**AII** was unchanged (Figure 1A); in contrast, cytosolic LC3**BI** did not change
256 in TG^{AC8}, whereas lipidated LC3**BII** was significantly downregulated, compared to WT
257 (Figure 1B). The ratio LC3II/LC3I, an indication of autophagy induction/activation, and of
258 LC3 processing efficiency, did not differ between genotypes. Specifically, it was
259 significantly decreased for both isoforms in TG^{AC8}, compared to WT, due to upregulation
260 of LC3**AI** and downregulation of LC3**BII**, respectively (Figures 1C, 1D). Moreover,
261 phosphorylation of LC3 at S12[27], which inhibits LC3 activity, was 50% reduced (Figure
262 1E), and phosphorylation of LC3 at T50[28], which increases LC3 activity, was 30%
263 increased (Figure 1F) in TG^{AC8} vs WT, suggesting a more favorable autophagic context
264 in TG^{AC8} vs WT.

265 Expression of total p62, an essential autophagy protein adaptor[29,30], was significantly
266 upregulated in TG^{AC8} vs WT (Figure 2A), and p62 was hyper-phosphorylated at S403
267 (p62-S403) (Figure 2B) and at S349 (p62-S349) (Figure 2C), compared to WT; the ratios
268 to total p62 protein of phospho-proteins at both sites, were also significantly elevated
269 (Figure 2D, 2E), indicating a higher “aggresome” disposal (phosphorylation at S403
270 increases affinity to ubiquitinated cargo[29], including depolarized mitochondria[31]), and
271 activation of defense mechanisms against oxidative stress (phosphorylation at S349
272 activates NRF2-pathway[32]) in the TG^{AC8} heart, at 3-4 months of age.

273 In summary, chronic cardiac-specific over-expression of AC8 upregulates key
274 markers of selective autophagy (clearance of misfolded proteins/aggregates and
275 activation of protection mechanisms against oxidative stress) in the TG^{AC8} LV at a young
276 age, and maintains heart health in the context of cAMP-induction of a cardiac workload
277 at this age[14].

278 **Lysosomal function is increased and autophagic flux is accelerated in the TG^{AC8}**
279 **heart at 3-4 months of age**

280 Our previous work had shown that protein levels of lysosomal cathepsins are
281 upregulated in the TG^{AC8} at 3-4 months of age[14]. Here, we quantified relative changes in
282 different cathepsins in the TG^{AC8} LV, compared to WT. Cathepsins Z and S were more
283 enriched in TG^{AC8}, whereas cathepsin L1 showed the least significant change (Figure 3A,
284 Supplemental Table). We next assessed lysosome function by measuring cathepsin L1
285 activity, which was significantly higher in TG^{AC8} vs WT (Figure 3B). This result, paired by
286 an increase in the lysosomal acid phosphatase, ACP2, by WB (Figure 3C), suggested an
287 overall higher lysosomal fitness (function) in TG^{AC8} compared to WT.

288 Since autophagy is a dynamic, multi-steps process, we next evaluated how the young
289 TG^{AC8} heart handles autophagic cargo, from its uptake to its disposal. We assessed
290 autophagic flux by inhibiting lysosomal function with chloroquine (CQ). Basal autophagy
291 (in non-fasting conditions) was not appreciably affected in WT by CQ treatment, as
292 changes did not occur in LC3 and p62 (Figures 4A-D, Figure 4E). This result was
293 expected, because basal autophagy is normally <u>undetectable</u> by WB; in contrast, both
294 LC3**AI** and LC3**BI** (Figures 4A, 4B) and p62 protein levels (Figure 4E) became
295 significantly reduced in the TG^{AC8} following CQ treatment, compared to saline, whereas
296 LC3**AII** and LC3**BII** remained unchanged. Thus, in contrast to WT, basal LC3II/LC3I ratios

297 (both A and B isoforms) (Figures 4C, 4D) became significantly increased following CQ, in
298 TG^{AC8}.

299 We next directly visualized autophagic figures in TG^{AC8} using transmission electron
300 microscopy (TEM). A significant increase in the numbers of both early and late autophagic
301 events (Figure 4F, 4G) was detected in TG^{AC8} vs WT, demonstrating that basal autophagy
302 differed by genotype, and that basal autophagic flux was accelerated in TG^{AC8}.

303 To summarize the results thus far, an accelerated autophagic flux and an increase in
304 lysosome performance ensures effective clearance of misfolded proteins, preventing
305 excessive insoluble protein "garbage" accumulation in the young (3-4 months) TG^{AC8}
306 heart. Thus, more efficient autophagy in TG^{AC8} occurs in the context of increased cardiac
307 workload and upregulation of aspects of cardiac protection circuitry, compared to WT at
308 this age[14].

309 **Accelerated autophagic flux of the youthful TG^{AC8} heart becomes insufficient in old**
310 **age**

311 Because autophagy induction and clearance have been shown to decrease with
312 aging[9], and TG^{AC8} mice develop cardiomyopathy at older ages[18], we next compared LC3
313 and ATG4B (involved in LC3 turnover)[33] in young and aged TG^{AC8} LVs and age-matched
314 WT. Both LC3 and ATG4B markers were significantly downregulated in both TG^{AC8} and
315 WT with aging (Figures 5A, 5B, Figure S1), with specific accumulation of LC3II (Figures
316 5A, 5B), compared to young animals. Upregulated levels of LC3II, with aging, increased
317 LC3II/LC3I ratios in both isoforms in both genotypes, and pointed to aging as the main
318 mechanism (Figures 5C, 5D, S2i, S2ii).

319 Paired TEM micrograph analysis (planimetry and stereology) showed a significant
320 age-associated decrease in event flux in *early* stages of autophagy (Figures 5E, 5I); in

321 contrast, *late*-stage event flux was increased (Figures 5H, 5I). This results, taken together
322 with the accumulation of lipidated LC3II, confirm an accelerated downregulation of
323 autophagy induction and impaired cargo clearance due to aging, per se, regardless of
324 genotype.

325 We next focused on autophagy and cargo disposal between the old TG^{AC8} and old
326 WT. We specifically assessed LC3 states (including phosphorylation) by WB, and
327 measured autophagic flux. Interestingly, LC3**AI** levels were significantly *upregulated* in
328 old TG^{AC8} compared to age-matched WT (Figures 6A), (similar to the genotypic difference
329 in LC3**AI** expression at 3-4 months (Figure 1A)); but LC3**AII** *did not* significantly differ by
330 genotype. Thus, LC3AII/LC3AI ratio was decreased in old TG^{AC8} vs WT (Figure S3i). In
331 contrast, LC3**BI** and LC3**BII** (Figures 6B), nor LC3BII/LC3BI ratio (Figure S3ii) did not
332 significantly differ by genotype in old age. Further, LC3 phosphorylation (S12 and T50)
333 and ACP2 protein levels at 21 months of age (Figure S4) also did not differ by genotype.
334 Taken together, these results indicate that autophagy declines with age, regardless of
335 genotype, and autophagic insufficiency in old age is greater in TG^{AC8} than in WT.

336 As expected, and similar to 3-4 month of WT, autophagic flux assessment in old WT
337 showed that basal levels of LC3 and p62 (in non-fasting conditions) did not differ following
338 CQ treatment. In old TG^{AC8}, however, both LC3**AI** and LC3**AII** significantly increased in
339 response to CQ vs WT-CQ (Figure 6A), leading to no change in LC3AII/LC3AI ratio
340 (Figure 6C); LC3**AII** also increased in response to CQ, compared to TG^{AC8}-saline, an
341 indication of a faster flux for LC3A in old TG^{AC8} vs WT. LC3B forms were not affected by
342 CQ in old TG^{AC8} (Figure 6B), but LC3BII/LC3BI ratio showed a trend to significantly
343 increase (Figure 6D), demonstrating that LC3 isoform-specific modulation persists in old

344 age, as previously observed in TG^{AC8} at the younger age. In line with these results, CQ
345 remarkably reduced p62 expression in old TG^{AC8} (Figure 6E) similarly to younger age
346 (Figure 4E), indicating a faster autophagic flux for p62, although *overall* autophagic flux
347 was indeed significantly reduced (Figure 6Fi, 6Fii).

348 Taken together, data in figures suggest that similar to 3-4 months of age, basal
349 autophagy and autophagic flux of LC3A and p62 autophagic markers remain accelerated
350 in old TG^{AC8}, compared to age-matched WT, but *overall* autophagic flux becomes slower
351 in old TG^{AC8} compared to old WT, and is clearly insufficient for proper protein garbage
352 clearance**.**

353 **More severely dysregulated proteostasis in the old TG^{AC8} heart leads to increased**
354 **cell "garbage" accumulation, disruption of the cardiac contractile machinery, and**
355 **exaggerated cardiac aging**

356 We next assessed translation rates and PQC mechanisms (UPS activity, aggregates
357 accumulation, and mitophagy) in young and aged TG^{AC8}, and age-matched WT. Our
358 previous work in young mice (3-4 months of age) demonstrated that: 1) the ubiquitin
359 proteasome system (UPS) and autophagy, including mitophagy, were all upregulated in
360 TG^{AC8}, compared to WT, indicating cooperation among PQC mechanisms[14]; 2) although
361 the protein synthesis rate was 40% higher in TG^{AC8} vs WT, UPS clearance of soluble
362 aggregates was also upregulated, and insoluble protein "garbage" did not accumulate
363 within cells[14]; 3) the numbers of healthy mitochondria and the percent of cell volume
364 occupied by them, did not differ between TG^{AC8} and WT[14]; and additionally, 4) although
365 the canonical cargo receptors PARKIN was significantly upregulated[14], mitochondrial
366 fitness was comparable between genotypes.

367 In contrast to younger age, proteasome activity did not increase in old TG^{AC8} (Figure
368 7A), compared to age-matched WT. However, UPS function in TG^{AC8} progressively
369 declined with aging, from 3-4 to 18 months, whereas it remained the same during aging
370 in WT controls (Figure 7A). The density of *soluble* aggregates also did not differ by
371 genotype, but it decreased with aging both in old TG^{AC8} and WT (Figure 7Bi). In contrast,
372 the ratio of insoluble to soluble aggregates significantly increased in TG^{AC8} from 3-4
373 months to 18 months, compared to the aging WT (Figure 7Bii), indicating the increased
374 accumulation of *insoluble* garbage material in the TG^{AC8} heart, during the aging process,
375 compared to "normal" aging WT.

376 The rate of protein synthesis in aged mice did not differ by genotype (Figure 7C).
377 However, protein translation rates significantly decreased in TG^{AC8}, from 3-4 to 18
378 months, a hallmark of aging in health[34].

379 Next, we evaluated mitophagy signaling pathways in aged TG^{AC8} and age-matched
380 WT by assessing the expression of specific cargo receptors involved in canonical and
381 non-canonical mitophagy pathways[35]. Similar to young TG^{AC8}, the canonical cargo
382 receptors PARKIN (Figure 7D), p62-S403 (Figure 7E), recruited to depolarized[31] and
383 polyubitiquinated[36] mitochondria, respectively, and p62-S349 (Figure 7F), upregulated in
384 conditions of oxidative stress[32], were all significantly increased in aged TG^{AC8} compared
385 to age-matched WT, suggesting that canonical mitophagy is incremented in TG^{AC8} vs WT.
386 However, the non-canonical cargo receptor FKBP8[37], which assists LC3A during
387 mitophagy and in the clearance of misfolded proteins, was also significantly *upregulated*
388 (Figure 7G) in the old TG^{AC8} vs WT, in contrast to young TG^{AC8} (Figure S6). This suggests
389 the concurrent activation of canonical and non-canonical mitophagy in old TG^{AC8}. But, in

390 spite of upregulation of both canonical and non-canonical mitophagy signaling in old
391 TG^{AC8}, staining of semi-thin TEM sections still revealed extensive accumulation of
392 undigested material, with also included disrupted mitochondrial structure (Figure 7H),
393 indicating that although signaling for garbage disposal is upregulated in old TG^{AC8}, overall
394 mitophagy fails, with the rate of mitochondrial degradation exceeding the rate of garbage
395 clearance.

396 Taken together, these results demonstrate that, although protein synthesis decreases
397 with aging, in TG^{AC8} compared to age-matched WT, to preserve energy and focus on
398 repair mechanisms, such as during the healthy aging process, PQC mechanisms become
399 progressively inefficient because of UPS insufficiency occurring in the context of a
400 maladaptive autophagic flux and a failing mitophagy, leading to more severe age-
401 associated dysregulated proteostasis in the old TG^{AC8} heart, compared to age-matched
402 WT.

403 To further assess the age-associated proteostasis dysregulation in old TG^{AC8} heart,
404 we evaluated the contribution of desmin to cardiac proteotoxicity in aged TG^{AC8},
405 compared to age-matched WT. Recent evidence has shown the contribution of desmin
406 filaments, which interlinks the contractile myofibrillar apparatus to mitochondria, nuclei
407 and the sarcolemma, to impaired mitochondrial fission[38] and proteostasis[38], and desmin
408 disorganization has been documented as a consequence of accumulation of preamyloid
409 oligomers (PAOs) aggregates in the heart[39]. TG^{AC8} had significantly higher levels of
410 desmin PAOs (Figure 8A), compared to WT. Moreover, a higher percentage of desmin
411 was tagged for ubiquitination (Figure 8Bi), and cleaved (Figure 8Bii), an indication of the

412 severe alteration of the myofilament ultrastructure in the old TG^{AC8} heart vs age-matched
413 WT.

414 We also evaluated the extent of accumulation of undigested material by performing
415 LF quantification by semi-thin staining assessment (TEM). There was no difference in
416 number (Figure 8C) or average size (Figure 8D) of LF bodies in old TG^{AC8} vs age-matched
417 WT. There was, however, a marked heterogeneity size within the LF population (Figure
418 8E, 8F) with increased total volume of LF and incremented individual LF body' sizes
419 (Figure 8G) in TG^{AC8}, compared to WT, covering, in some cases, a large percentage of
420 the cardiomyocyte area (Figure 8H). Interestingly, large insoluble aggregates displaying
421 different pigmentation (brownish to black) were only present in TG^{AC8} LVs (Figure 8I),
422 suggesting a different and/or denser composition.

423 Taken together, the disruption of the cardiac contractile machinery by desmin
424 disorganization and increased desmin PAOs, in tandem with the accumulation of the age
425 pigment LF and the heterogeneity of LF bodies, highly contribute to TG^{AC8} accelerated
426 aging, compared to age-matched WT.

427 DISCUSSION

428 Marked chronic catecholamine-induced cardiac stress leads to heart failure[21,40]. Our
429 previous work had shown that, at 3-4 months of age, numerous concentric adaptation
430 mechanisms protect TG^{AC8} heart health and function in response to sustained activation
431 of the AC/cAMP/PKA/Ca^{2+} axis[14]. Among other mechanisms, protein quality control,
432 including the UPS and the autophagic machinery, were upregulated in the TG^{AC8} heart.
433 The present study evaluated proteostasis in the TG^{AC8} heart more in detail, focusing on
434 key players involved in the autophagic process, and probed whether protein quality

435 control mechanisms remained upregulated in advanced age, compared to aging WT. Our
436 results reveal that in a context of chronic exposure (up to 17-21 to months) to marked
437 cardiac cAMP-induced stress, some PQC mechanisms fail more severely in TG^{AC8} than
438 in WT.

439 **Upregulation of specific components of autophagy at 3-4 months of age in the**
440 **TG^{AC8} heart**

441 Specifically, our results demonstrate that at 3-4 months of age the TG^{AC8} heart
442 upregulates the autophagic processes by fine tuning levels of key effectors such as LC3,
443 and its isoforms LCA and LC3B, which localize to different
444 phagophores/autophagosomes[26]. This suggests that efficient modulation of LC3's
445 isotype-specific functions[26] that guarantee effective clearance of damaged proteins, is
446 essential in a scenario of high cardiac workload and energy demand. Specifically, at 3-4
447 months of age, both LC3**AI** (the cytosolic form of LC3, which becomes lipidated to LC3II)
448 and LC3**BII** (the lipidated LC3I, which localizes on autophagosomes and
449 autophagolysosomes[41] during autophagy), differed in TG^{AC8} vs WT, in a scenario
450 indicative of upregulated autophagy. LC3**AI** *upregulation* in TG^{AC8} was both
451 transcriptional[14] and translational, and since LC3A, together with FKBP8, also increased
452 in TG^{AC8}, are important markers of mitophagy, we speculate that upregulation of both
453 LC3A and FKBP8 are important for efficient PQC in the stressed-out TG^{AC8} heart. The
454 significant LC3**BII** *downregulation* in TG^{AC8} vs age-matched WT, is consistent with the
455 idea that LC3A and LC3B are involved in different signaling pathways (mitophagy[42,43] vs
456 apoptosis[44] vs endosome-mediated autophagy[45,46]). LC3 post-translational modifications
457 (PTMs) by phosphorylation, that affect its activity[27,28], were also differentially modulated
458 in the young TG^{AC8} vs WT heart in a way that favored both *early* and *late* stages of

459 autophagy: specifically, phosphorylation of LC3 at S12 was significantly reduced,
460 whereas its phosphorylation at T50 was significantly increased. Phosphorylation at S12
461 by PKA/PKC[47] inhibits autophagy by preventing autophagosome wall elongation,
462 whereas phosphorylation at T50 by STK3/4[28] stimulates the autophagic process by
463 promoting autophagolysosome fusion.

464 p62/sequestosome-1, an essential autophagy adaptor protein[48] that colocalizes with
465 ubiquitin and LC3, was significantly upregulated in the young TG^{AC8} heart. p62 plays a
466 critical role in "aggresome" formation[49] and clearance[49] by activating autophagy.
467 Specifically, p62 recognizes cargo tagged for disposal (polyubiquitinated proteins,
468 cytosolic protein aggregates and cellular inclusion bodies, which are aggregates of
469 aggregates[50]) that accumulate with chronic stress, and in toxic and degenerative
470 conditions, and transports it to the lysosome[29,51], while, itself, becoming an autophagy
471 substrate[52]. Phospho-forms p62-S403 and p62-S349, and the ratios of phosphorylated
472 p62 to total p62, were also upregulated in TG^{AC8} vs WT at 3-4 months. Phosphorylation
473 of p62 at S403, increases its selectivity and affinity towards ubiquitin, and has been shown
474 to positively correlate to ubiquitinated cargo[53], including protein aggregates[54] and
475 polyubitiquinated mitochondria[53]. Phosphorylation of p62 at S349, in contrast, has a
476 higher affinity for the ubiquitin ligase adaptor Kelch-like ECH-associated protein 1
477 (KEAP1)[55], resulting in constitutive activation of the transcription factor NF-E2-related
478 factor 2 (NRF2) and regulation of its downstream signaling pathways[56]. Transient
479 accumulation of p62 bodies by upregulation of p62 and it phospho-forms in the young
480 TG^{AC8} heart, demonstrates its important role in the induction of autophagy[57], and in both
481 adaptation to the sequelae evoked by upregulation of signaling for protein aggregate

482 clearance, and increased ROS scavenging, a protection mechanism from oxidative stress
483 by sustained activation of the AC/cAMP/PKA/Ca^{2+} axis.

484 Overall autophagic flux in TG^{AC8} vs WT at 3-4 months was increased. Specifically, the
485 flux of LC3 and p62 markers was accelerated, as evidenced by the increased LC3II/LC3I
486 ratios following CQ treatment, because of accumulation of LC3II at the lysosome in TG^{AC8}
487 vs WT. In addition, cathepsin L1 activity was upregulated, and protein levels of the
488 lysosomal acid phosphatase ACP2 were higher in TG^{AC8}. This finding, together with the
489 results of our previous study showing increased proteasome activity without accumulation
490 of insoluble protein aggregates, and increased levels of proteins involved in the
491 autophagic machinery[14], demonstrate that UPS and autophagic pathways concurrently
492 operate in a more efficient mode in the young TG^{AC8} heart to manage its state of chronic,
493 marked cardiac cAMP-derived stress[58,59].

494 **PQC mechanisms in the TG^{AC8} vs WT at older age**

495 Autophagy markers LC3 and the autophagy related 4B cysteine peptidase (ATG4B),
496 involved in LC3 lifecycle[33], became significantly downregulated with aging, in both TG^{AC8}
497 and WT, indicating that cardiac aging, per se, negatively impacts on PQC. However,
498 assessment of autophagic flux revealed that flux of LC3A and p62 was *upregulated* in old
499 TG^{AC8}, compared to age-matched WT, but that *overall* autophagic flux was reduced in
500 TG^{AC8} as well as than in WT, as demonstrated by reduced numbers of early autophagy
501 figures, and an increased number of late autophagic events (by TEM quantification).

502 Accelerated autophagy marker flux has been shown to be a compensation
503 mechanism, that can be maladaptive in disease conditions that contribute to the
504 remodeling of the myocardium under stress[60]. We interpret the higher p62 flux within the
505 context of chronic upregulation of the AC/cAMP/PKA/Ca^{2+} axis in old TG^{AC8}, as a sensing

506 mechanism for the increased presence of “aggresomes”[50] (“aggregate of aggregates”
507 encaged by intermediate filament proteins[60,61]), the accumulation of which, in advanced
508 age, results from the buildup of numerous small preaggresomal bodies
509 compartmentalized at younger age as a cytoprotective mechanism[61,62].

510 Moreover, an accelerated LC3A flux may lead to an increased number of mitochondria
511 tagged for disposal, another index of garbage production/accumulation.

512 Although mitochondria carry out several critical and diverse functions[58],
513 cardiomyocytes have extremely high mitochondrial density because a steady production
514 and supply of adenosine triphosphate (ATP) via oxidative phosphorylation is required by
515 the heart, because of its continuous high demand for energy. It has been established,
516 however, that mitochondria and lysosomes of long-lived cells such as cardiac myocytes
517 suffer remarkable age-related alterations as the machinery of cellular protein turnover
518 becomes inherently more imperfect[63] as age advances. continuous Mitochondrial
519 changes, by physiological oxidative stress[63] and increased reactive oxygen species
520 (ROS) production, include structural disorganization and enlargement, while lysosomes,
521 which are responsible for autophagic turnover of mitochondria, accumulate LF (age
522 pigment), a polymeric, autofluorescent, undegradable material, mainly composed of
523 proteins and lipids[64]. Damaged and/or dysfunctional mitochondria[2,59] are unable to
524 support high energy demands, and overall mitochondrial fitness declines, deterioration of
525 heart function leads to disease conditions.

526 The cooperation of LC3A with the non-canonical mitophagy receptor FKBP8, assigns
527 a new important role to LC3A in mitophagy and the process of mitochondrial turnover,
528 rendering LC3A an important informant of mitochondrial fitness, in adult cardiac tissue[42].

529 In old TG^{AC8}, all mitophagy pathways were activated, compared to age-matched WT
530 controls. However, a faster LC3A flux, together with upregulated mitophagy signaling
531 through a variety of pathways[65] suggests that mitophagy fails to greater extent in TG^{AC8}
532 vs WT, resulting in poor mitochondrial fitness/function in TG^{AC8}, possibly due to
533 insufficient lysosomal activity.

534 Mitochondrial structure (assessed by semi-thin stain by TEM) was severely damaged
535 in old TG^{AC8}, accompanied by a significant increase and more aberrant accumulation of
536 LF bodies with increased size, and a distribution covering a higher percentage of
537 cardiomyocyte area vs old WT. LF aggregates cannot be removed from the cytosol by
538 the UPS[66], because they are covalently cross-linked aggregates, and their accumulation
539 at the later stage of autophagy is an indication of lysosomal impairment[67], which, together
540 with their known accumulation with advancing age, per se, suggests that the old TG^{AC8}
541 portrays a phenotype of accelerated cardiac aging compared to age-matched WT. In
542 addition, the brown to black pigment aggregates, in older TG^{AC8}, but not in age-matched
543 WT, suggests changes in cargo processing, and accumulation of different LV material in
544 TG^{AC8} vs WT.

545 In addition to failure at the lysosome, variations in UPS activity and expression,
546 reflecting age-associated metabolic, functional, or simply structural changes, may occur
547 in response to the different demands for the turnover of signaling and structural proteins.
548 Specifically, cardiac proteasomal insufficiency has been linked to accumulation of
549 "aggresomes", leading to partial disorganization of protein filaments [60,61], that are
550 displaced from their normal cellular distribution[50]. Disorganization of desmin filaments that
551 interlink the contractile myofibrillar apparatus with mitochondria, nuclei and the

552 sarcolemma, have been shown to affect mitochondrial positioning, therefore
553 compromising mitochondrial function, and leading to cardiomyocyte dysfunction[38,68].
554 Negative modulation of desmin's physical properties and assembly by its PTMs leads to
555 the build-up of cardiac preamiloyd oligomers (PAOs) and has been recently indicated to
556 be an index of premature and acquired heart failure (as occurred in TG^{AC8} at 18 months).
557 We evaluated desmin structure, and quantified accumulation of cardiac PAOs, in old
558 TG^{AC8}. Desmin was significantly tagged for ubiquitination and cleaved, and desmin PAOs
559 accumulation was also highly increased.in old TG^{AC8} heart, compared to age-matched
560 WT.

561 Although translation rates did not differ between genotypes at older ages, protein
562 synthesis significantly decreased more with aging in TG^{AC8} heart at 19-months compared
563 to 3-4-months, in accordance with a "normal" aging process[34,69] in TG^{AC8}. We interpret
564 this to indicate that, exactly as the age-matched WT, the old TG^{AC8} heart reduces energy
565 use and load on the protein quality control machinery, by directing proteases and
566 chaperons activity towards repair of existing proteins rather than the folding of new
567 ones[34,69,70]. Thus, the old TG^{AC8} heart utilizes a mechanism that preserves and increases,
568 life span as in healthy aging[70], to optimize energy use by reducing the formation of *de-*
569 *novo* proteins, in order to focus on repairing the existing proteome.

570 In line with these results, although *proteasome activity* did not differ between
571 genotypes *at* 18 months, between 3-4 months and 18 months, proteasome function
572 progressively declined in TG^{AC8} but not in WT, leading to increased accumulation of
573 insoluble misfolded proteins. As a result, soluble aggregates (soluble proteins undergoing
574 normal turnover and misfolded proteins *en route* to degradation by the UPS), became

575 significantly reduced in *both* genotypes at 18 months. We interpret this result to indicate
576 that protein insolubility increases with age, per se, and that, with aging, misfolded proteins
577 are more "aggregate-prone"[50]. Thus, the presence of high molecular weight oligomers[50],
578 more stable than the intermediate conformers from which they are derived, clearly
579 demonstrate that the proteasome of the old TG^{AC8} heart is "out-won" in the competition
580 for misfolded substrates prior to their aggregation[71].

581 Thus, in the older TG^{AC8} proteasomal insufficiency in a context of a faster autophagy
582 flux indicates the overall presence of maladaptive responses with ineffective cargo
583 clearance, as has been previously demonstrated in hearts or cardiomyocytes under
584 disease and pathological conditions[72], including desminopathy[60]. In other terms, we
585 interpret our result to indicate that severe loss of proteostasis in the old TG^{AC8} heart
586 compared to age-matched WT, due to loss of PQC.

587 In conclusion, in response to chronic cardiac AC-dependent cAMP-stress that
588 activates protective concentric signaling circuitry, including autophagic flux, proteasome
589 activity and maintains PQC that preserve heart health early in life[14], with age, although
590 overall autophagy remained accelerated in TG^{AC8}, insufficient proteasomal activity
591 compromising PQC, contributed to accelerated cardiac aging and reduced cardiac health
592 span, that leads to age-associated cardiomyopathy[15] in TG^{AC8}.

593

ACKNOWLEDGMENTS

The study was designed by M.G.P. and E.G.L. The experiments were conducted by M.G.P., M.C.B., G.A., H.K., M.R., A.P., D.R.R., K.T., and K.C. The data were analyzed by M.G.P., M.C.B., G.A., C.H.M., and J.Q. The article was written by M.G.P. and E.G.L., and approved by all authors.

SOURCES OF FUNDING

This research was supported entirely by the Intramural Research Program of the NIH, National Institute on Aging (USA).

DISCLOSURES

None.

REFERENCES

1. Taylor RC, Dillin A. Aging as an event of proteostasis collapse. *Cold Spring Harb Perspect Biol*. 2011;3. doi: 10.1101/cshperspect.a004440
2. Linton PJ, Gurney M, Sengstock D, Mentzer RM, Jr., Gottlieb RA. This old heart: Cardiac aging and autophagy. *J Mol Cell Cardiol*. 2015;83:44-54. doi: 10.1016/j.yjmcc.2014.12.017
3. Kholova I, Niessen HW. Amyloid in the cardiovascular system: a review. *J Clin Pathol*. 2005;58:125-133. doi: 10.1136/jcp.2004.017293
4. Agnetti G, Halperin VL, Kirk JA, Chakir K, Guo Y, Lund L, Nicolini F, Gherli T, Guarnieri C, Caldarera CM, et al. Desmin modifications associate with amyloid-like oligomers deposition in heart failure. *Cardiovasc Res*. 2014;102:24-34. doi: 10.1093/cvr/cvu003
5. Sanbe A, Osinska H, Saffitz JE, Glabe CG, Kayed R, Maloyan A, Robbins J. Desmin-related cardiomyopathy in transgenic mice: a cardiac amyloidosis. *Proc Natl Acad Sci U S A*. 2004;101:10132-10136. doi: 10.1073/pnas.0401900101
6. Del Monte F, Agnetti G. Protein post-translational modifications and misfolding: new concepts in heart failure. *Proteomics Clin Appl*. 2014;8:534-542. doi: 10.1002/prca.201400037
7. Rainer PP, Dong P, Sorge M, Fert-Bober J, Holewinski RJ, Wang Y, Foss CA, An SS, Baracca A, Solaini G, et al. Desmin Phosphorylation Triggers Preamyloid Oligomers Formation and Myocyte Dysfunction in Acquired Heart Failure. *Circ Res*. 2018;122:e75-e83. doi: 10.1161/CIRCRESAHA.117.312082
8. Mizushima N, Levine B, Cuervo AM, Klionsky DJ. Autophagy fights disease through cellular self-digestion. *Nature*. 2008;451:1069-1075. doi: 10.1038/nature06639
9. Wilhelm T, Richly H. Autophagy during ageing - from Dr Jekyll to Mr Hyde. *FEBS J*. 2018;285:2367-2376. doi: 10.1111/febs.14453

627 10. Marzabadi MR, Sohal RS, Brunk UT. Mechanisms of lipofuscinogenesis: effect of the inhibition of
628 lysosomal proteinases and lipases under varying concentrations of ambient oxygen in cultured rat
629 neonatal myocardial cells. *APMIS*. 1991;99:416-426. doi: 10.1111/j.1699-0463.1991.tb05170.x
630 11. Lopez-Otin C, Blasco MA, Partridge L, Serrano M, Kroemer G. Hallmarks of aging: An expanding
631 universe. *Cell*. 2023;186:243-278. doi: 10.1016/j.cell.2022.11.001
632 12. Munnell JF, Getty R. Rate of accumulation of cardiac lipofuscin in the aging canine. *J Gerontol*.
633 1968;23:154-158. doi: 10.1093/geronj/23.2.154
634 13. Nakano M, Oenzil F, Mizuno T, Gotoh S. Age-related changes in the lipofuscin accumulation of
635 brain and heart. *Gerontology*. 1995;41 Suppl 2:69-79. doi: 10.1159/000213726
636 14. Tarasov KV, Chakir K, Riordon DR, Lyashkov AE, Ahmet I, Perino MG, Silvester AJ, Zhang J, Wang
637 M, Lukyanenko YO, et al. A remarkable adaptive paradigm of heart performance and protection
638 emerges in response to marked cardiac-specific overexpression of ADCY8. *Elife*. 2022;11. doi:
639 10.7554/eLife.80949
640 15. Lipskaia L, Defer N, Esposito G, Hajar I, Garel MC, Rockman HA, Hanoune J. Enhanced cardiac
641 function in transgenic mice expressing a Ca(2+)-stimulated adenylyl cyclase. *Circ Res*.
642 2000;86:795-801. doi: 10.1161/01.res.86.7.795
643 16. Georget M, Mateo P, Vandecasteele G, Jurevicius J, Lipskaia L, Defer N, Hanoune J, Hoerter J,
644 Fischmeister R. Augmentation of cardiac contractility with no change in L-type Ca2+ current in
645 transgenic mice with a cardiac-directed expression of the human adenylyl cyclase type 8 (AC8).
646 *FASEB J*. 2002;16:1636-1638. doi: 10.1096/fj.02-0292fje
647 17. Georget M, Mateo P, Vandecasteele G, Lipskaia L, Defer N, Hanoune J, Hoerter J, Lugnier C,
648 Fischmeister R. Cyclic AMP compartmentation due to increased cAMP-phosphodiesterase activity
649 in transgenic mice with a cardiac-directed expression of the human adenylyl cyclase type 8 (AC8).
650 *FASEB J*. 2003;17:1380-1391. doi: 10.1096/fj.02-0784com
651 18. Mougenot N, Mika D, Czibik G, Marcos E, Abid S, Houssaini A, Vallin B, Guellich A, Mehel H, Sawaki
652 D, et al. Cardiac adenylyl cyclase overexpression precipitates and aggravates age-related
653 myocardial dysfunction. *Cardiovasc Res*. 2019;115:1778-1790. doi: 10.1093/cvr/cvy306
654 19. Liu Y, Zhou K, Li J, Agvanian S, Caldaruse AM, Shaw S, Hitzeman TC, Shaw RM, Hong T. In Mice
655 Subjected to Chronic Stress, Exogenous cBIN1 Preserves Calcium-Handling Machinery and Cardiac
656 Function. *JACC Basic Transl Sci*. 2020;5:561-578. doi: 10.1016/j.jacbts.2020.03.006
657 20. Zhang GX, Kimura S, Nishiyama A, Shokoji T, Rahman M, Yao L, Nagai Y, Fujisawa Y, Miyatake A,
658 Abe Y. Cardiac oxidative stress in acute and chronic isoproterenol-infused rats. *Cardiovasc Res*.
659 2005;65:230-238. doi: 10.1016/j.cardiores.2004.08.013
660 21. Moen JM, Matt MG, Ramirez C, Tarasov KV, Chakir K, Tarasova YS, Lukyanenko Y, Tsutsui K,
661 Monfredi O, Morrell CH, et al. Overexpression of a Neuronal Type Adenylyl Cyclase (Type 8) in
662 Sinoatrial Node Markedly Impacts Heart Rate and Rhythm. *Front Neurosci*. 2019;13:615. doi:
663 10.3389/fnins.2019.00615
664 22. Kayed R, Head E, Thompson JL, McIntire TM, Milton SC, Cotman CW, Glabe CG. Common structure
665 of soluble amyloid oligomers implies common mechanism of pathogenesis. *Science*.
666 2003;300:486-489. doi: 10.1126/science.1079469
667 23. Weibel ER. *Stereological methods*. London ; New York: Academic Press; 1979.
668 24. Palade GE. A study of fixation for electron microscopy. *J Exp Med*. 1952;95:285-298. doi:
669 10.1084/jem.95.3.285
670 25. Ferreira JA, Zwinderman AH. On the Benjamini-Hochberg method. *Ann Stat*. 2006;34:1827-1849.
671 doi: 10.1214/009053606000000425
672 26. Koukourakis MI, Kalamida D, Giatromanolaki A, Zois CE, Sivridis E, Pouliliou S, Mitrakas A, Gatter
673 KC, Harris AL. Autophagosome Proteins LC3A, LC3B and LC3C Have Distinct Subcellular

674 Distribution Kinetics and Expression in Cancer Cell Lines. *PLoS One*. 2015;10:e0137675. doi:
675 10.1371/journal.pone.0137675
676 27. Cherra SJ, 3rd, Kulich SM, Uechi G, Balasubramani M, Mountzouris J, Day BW, Chu CT. Regulation
677 of the autophagy protein LC3 by phosphorylation. *J Cell Biol*. 2010;190:533-539. doi:
678 10.1083/jcb.201002108
679 28. Wilkinson DS, Jariwala JS, Anderson E, Mitra K, Meisenhelder J, Chang JT, Ideker T, Hunter T, Nizet
680 V, Dillin A, et al. Phosphorylation of LC3 by the Hippo kinases STK3/STK4 is essential for autophagy.
681 *Mol Cell*. 2015;57:55-68. doi: 10.1016/j.molcel.2014.11.019
682 29. Lamark T, Svenning S, Johansen T. Regulation of selective autophagy: the p62/SQSTM1 paradigm.
683 *Essays Biochem*. 2017;61:609-624. doi: 10.1042/EBC20170035
684 30. Katsuragi Y, Ichimura Y, Komatsu M. p62/SQSTM1 functions as a signaling hub and an autophagy
685 adaptor. *FEBS J*. 2015;282:4672-4678. doi: 10.1111/febs.13540
686 31. Narendra D, Tanaka A, Suen DF, Youle RJ. Parkin is recruited selectively to impaired mitochondria
687 and promotes their autophagy. *J Cell Biol*. 2008;183:795-803. doi: 10.1083/jcb.200809125
688 32. Jain A, Lamark T, Sjottem E, Larsen KB, Awuh JA, Overvatn A, McMahon M, Hayes JD, Johansen T.
689 p62/SQSTM1 is a target gene for transcription factor NRF2 and creates a positive feedback loop
690 by inducing antioxidant response element-driven gene transcription. *J Biol Chem*.
691 2010;285:22576-22591. doi: 10.1074/jbc.M110.118976
692 33. Scherz-Shouval R, Shvets E, Fass E, Shorer H, Gil L, Elazar Z. Reactive oxygen species are essential
693 for autophagy and specifically regulate the activity of Atg4. *EMBO J*. 2007;26:1749-1760. doi:
694 10.1038/sj.emboj.7601623
695 34. Anisimova AS, Meerson MB, Gerashchenko MV, Kulakovskiy IV, Dmitriev SE, Gladyshev VN.
696 Multifaceted deregulation of gene expression and protein synthesis with age. *Proc Natl Acad Sci*
697 *U S A*. 2020;117:15581-15590. doi: 10.1073/pnas.2001788117
698 35. Moyzis A, Gustafsson AB. Multiple recycling routes: Canonical vs. non-canonical mitophagy in the
699 heart. *Biochim Biophys Acta Mol Basis Dis*. 2019;1865:797-809. doi: 10.1016/j.bbadis.2018.09.034
700 36. Matsumoto G, Shimogori T, Hattori N, Nukina N. TBK1 controls autophagosomal engulfment of
701 polyubiquitinated mitochondria through p62/SQSTM1 phosphorylation. *Hum Mol Genet*.
702 2015;24:4429-4442. doi: 10.1093/hmg/ddv179
703 37. Misaka T, Murakawa T, Nishida K, Omori Y, Taneike M, Omiya S, Molenaar C, Uno Y, Yamaguchi
704 O, Takeda J, et al. FKBP8 protects the heart from hemodynamic stress by preventing the
705 accumulation of misfolded proteins and endoplasmic reticulum-associated apoptosis in mice. *J*
706 *Mol Cell Cardiol*. 2018;114:93-104. doi: 10.1016/j.yjmcc.2017.11.004
707 38. Alam S, Abdullah CS, Aishwarya R, Miriyala S, Panchatcharam M, Peretik JM, Orr AW, James J,
708 Robbins J, Bhuiyan MS. Aberrant Mitochondrial Fission Is Maladaptive in Desmin Mutation-
709 Induced Cardiac Proteotoxicity. *J Am Heart Assoc*. 2018;7. doi: 10.1161/JAHA.118.009289
710 39. Agnetti G, Herrmann H, Cohen S. New roles for desmin in the maintenance of muscle homeostasis.
711 *FEBS J*. 2022;289:2755-2770. doi: 10.1111/febs.15864
712 40. Zhang X, Szeto C, Gao E, Tang M, Jin J, Fu Q, Makarewich C, Ai X, Li Y, Tang A, et al. Cardiotoxic
713 and cardioprotective features of chronic beta-adrenergic signaling. *Circ Res*. 2013;112:498-509.
714 doi: 10.1161/CIRCRESAHA.112.273896
715 41. Tanida I, Minematsu-Ikeguchi N, Ueno T, Kominami E. Lysosomal turnover, but not a cellular level,
716 of endogenous LC3 is a marker for autophagy. *Autophagy*. 2005;1:84-91. doi:
717 10.4161/auto.1.2.1697
718 42. Bhujabal Z, Birgisdottir AB, Sjottem E, Brenne HB, Overvatn A, Habisov S, Kirkin V, Lamark T,
719 Johansen T. FKBP8 recruits LC3A to mediate Parkin-independent mitophagy. *EMBO Rep*.
720 2017;18:947-961. doi: 10.15252/embr.201643147

721 43. Chu CT, Bayir H, Kagan VE. LC3 binds externalized cardiolipin on injured mitochondria to signal
722 mitophagy in neurons: implications for Parkinson disease. *Autophagy*. 2014;10:376-378. doi:
723 10.4161/auto.27191
724 44. Satyavarapu EM, Das R, Mandal C, Mukhopadhyay A, Mandal C. Autophagy-independent
725 induction of LC3B through oxidative stress reveals its non-canonical role in anoikis of ovarian
726 cancer cells. *Cell Death Dis*. 2018;9:934. doi: 10.1038/s41419-018-0989-8
727 45. Kondylis V, van Nispen Tot Pannerden HE, van Dijk S, Ten Broeke T, Wubbolts R, Geerts WJ, Seinen
728 C, Mutis T, Heijnen HF. Endosome-mediated autophagy: an unconventional MIIC-driven
729 autophagic pathway operational in dendritic cells. *Autophagy*. 2013;9:861-880. doi:
730 10.4161/auto.24111
731 46. Magne J, Green DR. LC3-associated endocytosis and the functions of Rubicon and ATG16L1. *Sci*
732 *Adv*. 2022;8:eabo5600. doi: 10.1126/sciadv.abo5600
733 47. Jiang H, Cheng D, Liu W, Peng J, Feng J. Protein kinase C inhibits autophagy and phosphorylates
734 LC3. *Biochem Biophys Res Commun*. 2010;395:471-476. doi: 10.1016/j.bbrc.2010.04.030
735 48. Rusten TE, Stenmark H. p62, an autophagy hero or culprit? *Nat Cell Biol*. 2010;12:207-209. doi:
736 10.1038/ncb0310-207
737 49. Pankiv S, Clausen TH, Lamark T, Brech A, Bruun JA, Outzen H, Overvatn A, Bjorkoy G, Johansen T.
738 p62/SQSTM1 binds directly to Atg8/LC3 to facilitate degradation of ubiquitinated protein
739 aggregates by autophagy. *J Biol Chem*. 2007;282:24131-24145. doi: 10.1074/jbc.M702824200
740 50. Kopito RR. Aggresomes, inclusion bodies and protein aggregation. *Trends Cell Biol*. 2000;10:524-
741 530. doi: 10.1016/s0962-8924(00)01852-3
742 51. Johansen T, Lamark T. Selective autophagy mediated by autophagic adapter proteins. *Autophagy*.
743 2011;7:279-296. doi: 10.4161/auto.7.3.14487
744 52. Bjorkoy G, Lamark T, Brech A, Outzen H, Perander M, Overvatn A, Stenmark H, Johansen T.
745 p62/SQSTM1 forms protein aggregates degraded by autophagy and has a protective effect on
746 huntingtin-induced cell death. *J Cell Biol*. 2005;171:603-614. doi: 10.1083/jcb.200507002
747 53. Matsumoto G, Wada K, Okuno M, Kurosawa M, Nukina N. Serine 403 phosphorylation of
748 p62/SQSTM1 regulates selective autophagic clearance of ubiquitinated proteins. *Mol Cell*.
749 2011;44:279-289. doi: 10.1016/j.molcel.2011.07.039
750 54. Lim J, Lachenmayer ML, Wu S, Liu W, Kundu M, Wang R, Komatsu M, Oh YJ, Zhao Y, Yue Z.
751 Proteotoxic stress induces phosphorylation of p62/SQSTM1 by ULK1 to regulate selective
752 autophagic clearance of protein aggregates. *PLoS Genet*. 2015;11:e1004987. doi:
753 10.1371/journal.pgen.1004987
754 55. Ichimura Y, Waguri S, Sou YS, Kageyama S, Hasegawa J, Ishimura R, Saito T, Yang Y, Kouno T,
755 Fukutomi T, et al. Phosphorylation of p62 activates the Keap1-Nrf2 pathway during selective
756 autophagy. *Mol Cell*. 2013;51:618-631. doi: 10.1016/j.molcel.2013.08.003
757 56. Jiang T, Harder B, Rojo de la Vega M, Wong PK, Chapman E, Zhang DD. p62 links autophagy and
758 Nrf2 signaling. *Free Radic Biol Med*. 2015;88:199-204. doi: 10.1016/j.freeradbiomed.2015.06.014
759 57. Szeto J, Kaniuk NA, Canadien V, Nisman R, Mizushima N, Yoshimori T, Bazett-Jones DP, Brumell
760 JH. ALIS are stress-induced protein storage compartments for substrates of the proteasome and
761 autophagy. *Autophagy*. 2006;2:189-199. doi: 10.4161/auto.2731
762 58. McBride HM, Neuspiel M, Wasiak S. Mitochondria: more than just a powerhouse. *Curr Biol*.
763 2006;16:R551-560. doi: 10.1016/j.cub.2006.06.054
764 59. Gottlieb RA, Carreira RS. Autophagy in health and disease. 5. Mitophagy as a way of life. *Am J*
765 *Physiol Cell Physiol*. 2010;299:C203-210. doi: 10.1152/ajpcell.00097.2010
766 60. Zheng Q, Su H, Ranek MJ, Wang X. Autophagy and p62 in cardiac proteinopathy. *Circ Res*.
767 2011;109:296-308. doi: 10.1161/CIRCRESAHA.111.244707

768 61. Garcia-Mata R, Gao YS, Sztul E. Hassles with taking out the garbage: aggravating aggresomes.
769 *Traffic*. 2002;3:388-396. doi: 10.1034/j.1600-0854.2002.30602.x
770 62. Johnston JA, Ward CL, Kopito RR. Aggresomes: a cellular response to misfolded proteins. *J Cell*
771 *Biol*. 1998;143:1883-1898. doi: 10.1083/jcb.143.7.1883
772 63. Terman A, Brunk UT. The aging myocardium: roles of mitochondrial damage and lysosomal
773 degradation. *Heart Lung Circ*. 2005;14:107-114. doi: 10.1016/j.hlc.2004.12.023
774 64. Konig J, Ott C, Hugo M, Jung T, Bulteau AL, Grune T, Hohn A. Mitochondrial contribution to
775 lipofuscin formation. *Redox Biol*. 2017;11:673-681. doi: 10.1016/j.redox.2017.01.017
776 65. Moyzis AG, Sadoshima J, Gustafsson AB. Mending a broken heart: the role of mitophagy in
777 cardioprotection. *Am J Physiol Heart Circ Physiol*. 2015;308:H183-192. doi:
778 10.1152/ajpheart.00708.2014
779 66. Hohn A, Jung T, Grimm S, Catalgol B, Weber D, Grune T. Lipofuscin inhibits the proteasome by
780 binding to surface motifs. *Free Radic Biol Med*. 2011;50:585-591. doi:
781 10.1016/j.freeradbiomed.2010.12.011
782 67. Hohn A, Sittig A, Jung T, Grimm S, Grune T. Lipofuscin is formed independently of macroautophagy
783 and lysosomal activity in stress-induced prematurely senescent human fibroblasts. *Free Radic Biol*
784 *Med*. 2012;53:1760-1769. doi: 10.1016/j.freeradbiomed.2012.08.591
785 68. Bar H, Strelkov SV, Sjoberg G, Aebi U, Herrmann H. The biology of desmin filaments: how do
786 mutations affect their structure, assembly, and organisation? *J Struct Biol*. 2004;148:137-152. doi:
787 10.1016/j.jsb.2004.04.003
788 69. Anisimova AS, Alexandrov AI, Makarova NE, Gladyshev VN, Dmitriev SE. Protein synthesis and
789 quality control in aging. *Aging (Albany NY)*. 2018;10:4269-4288. doi: 10.18632/aging.101721
790 70. Hipkiss AR. On why decreasing protein synthesis can increase lifespan. *Mech Ageing Dev*.
791 2007;128:412-414. doi: 10.1016/j.mad.2007.03.002
792 71. DiLoreto R, Murphy CT. The cell biology of aging. *Mol Biol Cell*. 2015;26:4524-4531. doi:
793 10.1091/mbc.E14-06-1084
794 72. Day SM. The ubiquitin proteasome system in human cardiomyopathies and heart failure. *Am J*
795 *Physiol Heart Circ Physiol*. 2013;304:H1283-1293. doi: 10.1152/ajpheart.00249.2012
796

GRAPHIC ABSTRACT/DIAGRAM

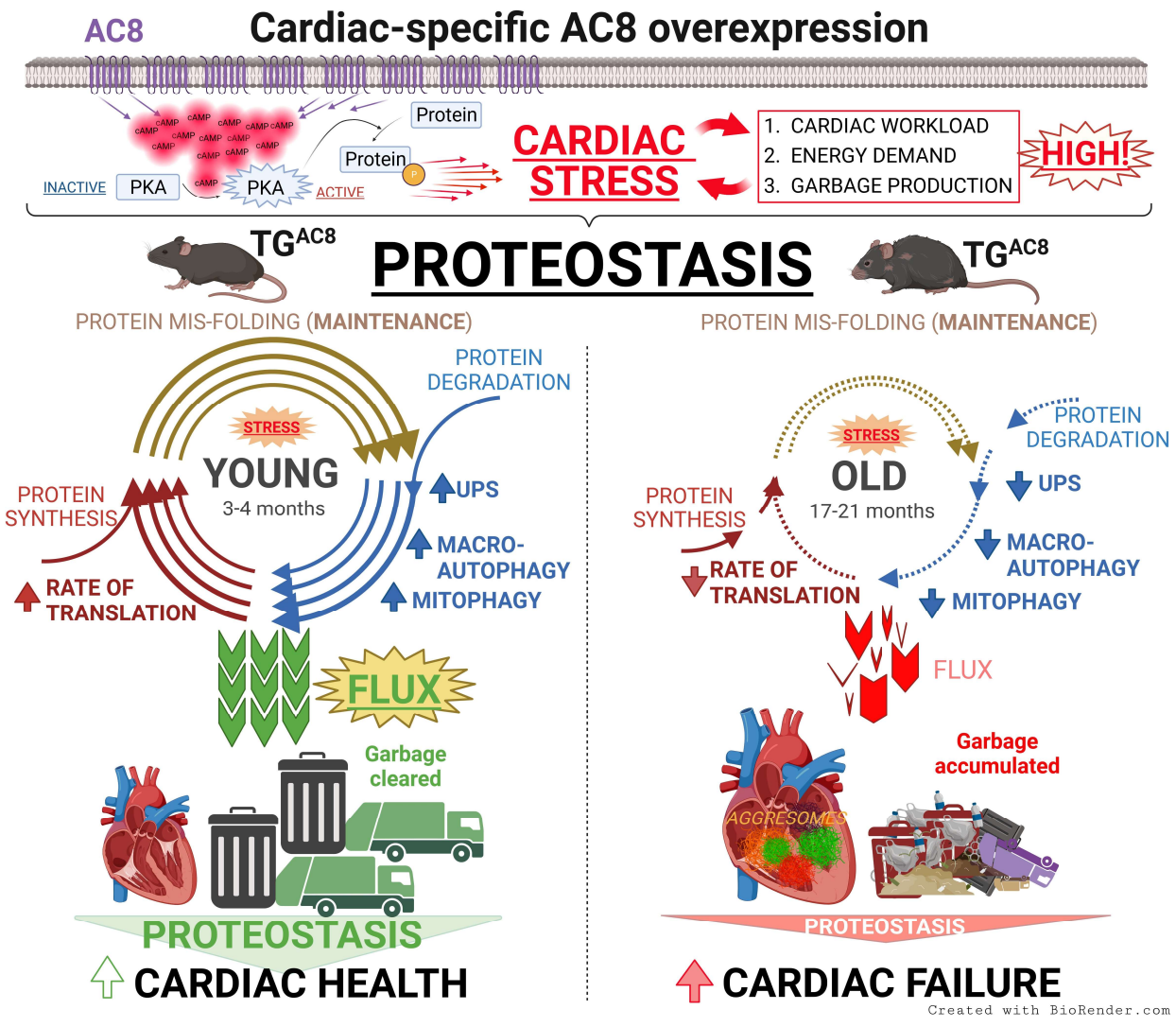

Table. Proteostasis in young and aged TG^{AC8} in the context of cardiac stress in response to cardiac-specific constitutive stimulation of the AC/cAMP/PKA/Ca^{2+} axis by α-MHC-driven AC8 overexpression.

802 # FIGURES WITH FIGURE LEGENDS

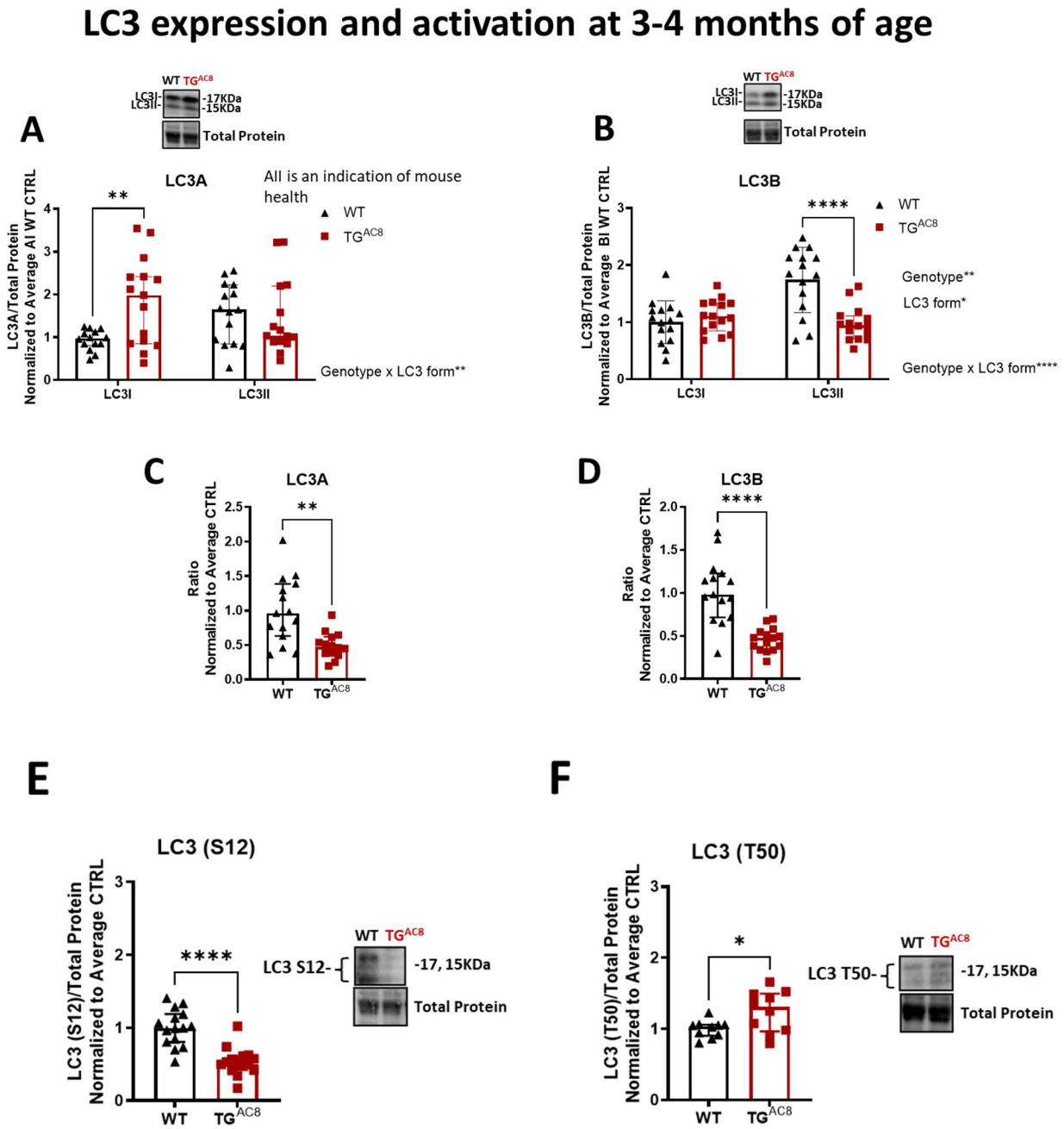

803

804

805 **Figure 1. LC3 isoforms are differently modulated in TG^{AC8} at 3-4 months of age, and**
806 **autophagy is promoted.**

807 Bar graphs and Western blot analysis of autophagy markers LC3, LC3II/LC3I ratios, and
808 LC3 phosphorylation in young TG^{AC8} LV and wild type (WT) at 3-3 months of age (n=15

mice per group). Data are presented as the median ± interquartile range **A**), LC3A; **B**), LC3B; **C**), LC3AII/LC3AI; **D**), LC3BII/LC3BI; **E**), LC3-S12; **F**), LC3-T50. **A and B**, A mixed-effect model for repeated measurements, followed by Original FDR method of Benjamini and Hochberg post-hoc multi-comparison test was used. **C, D, E and F**, Unpaired 2-tailed Students tests with Welch's correction was used. * indicates significant (<0.05) differences between genotypes (WT vs TG^{AC8}).

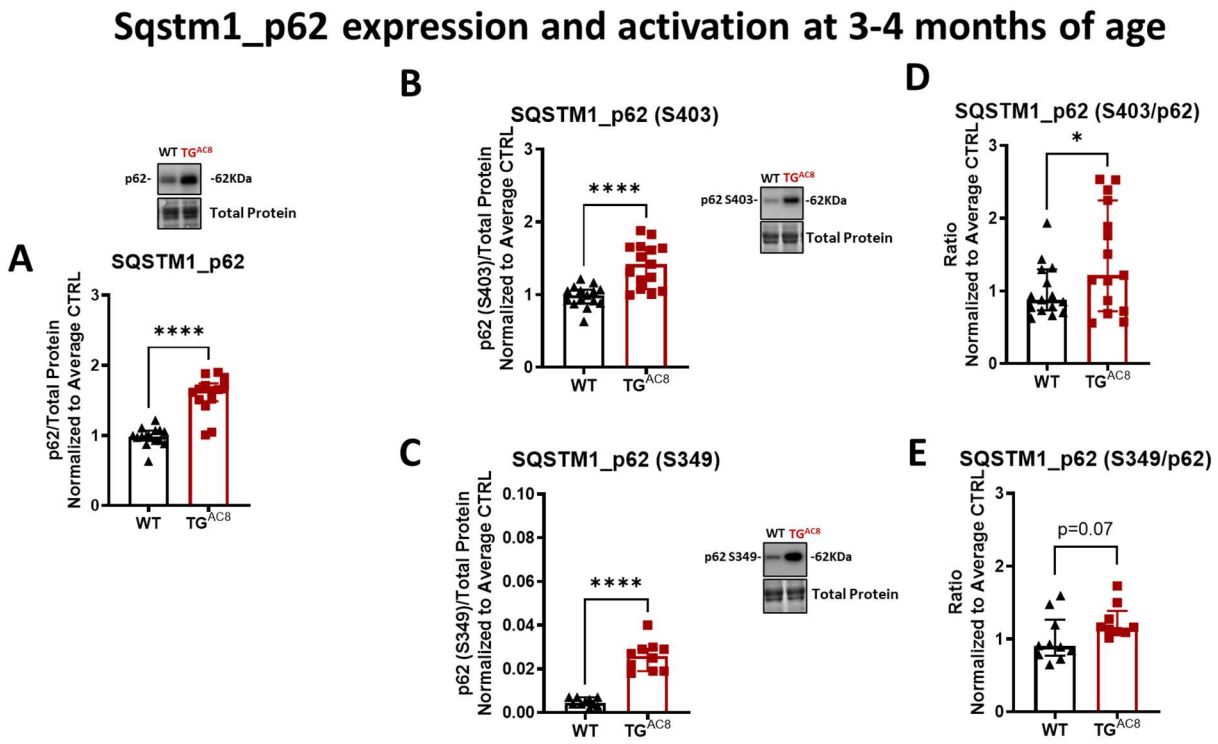

Figure 2. p62/sequestosome1 expression and phosphorylation are increased in TG^{AC8} at 3-4 months of age.

Bar graphs and Western blot analysis of the autophagy cargo receptor sequestosome1/p62, its post-translational modifications, and their ratios to total p62 in TG^{AC8} and WT at 3 months of age (n=15 mice per group). **A**), Total p62; **B**), p62-S403; **C**), p62-S349; **D**), p62-S403/p62; **E**), p62-S349/p62. Unpaired 2-tailed Student t test with

822 Welch's correction was used and data are presented as the median ± interquartile range.

823 * indicates significant differences (<0.05) between genotypes (WT vs TG^{AC8}).

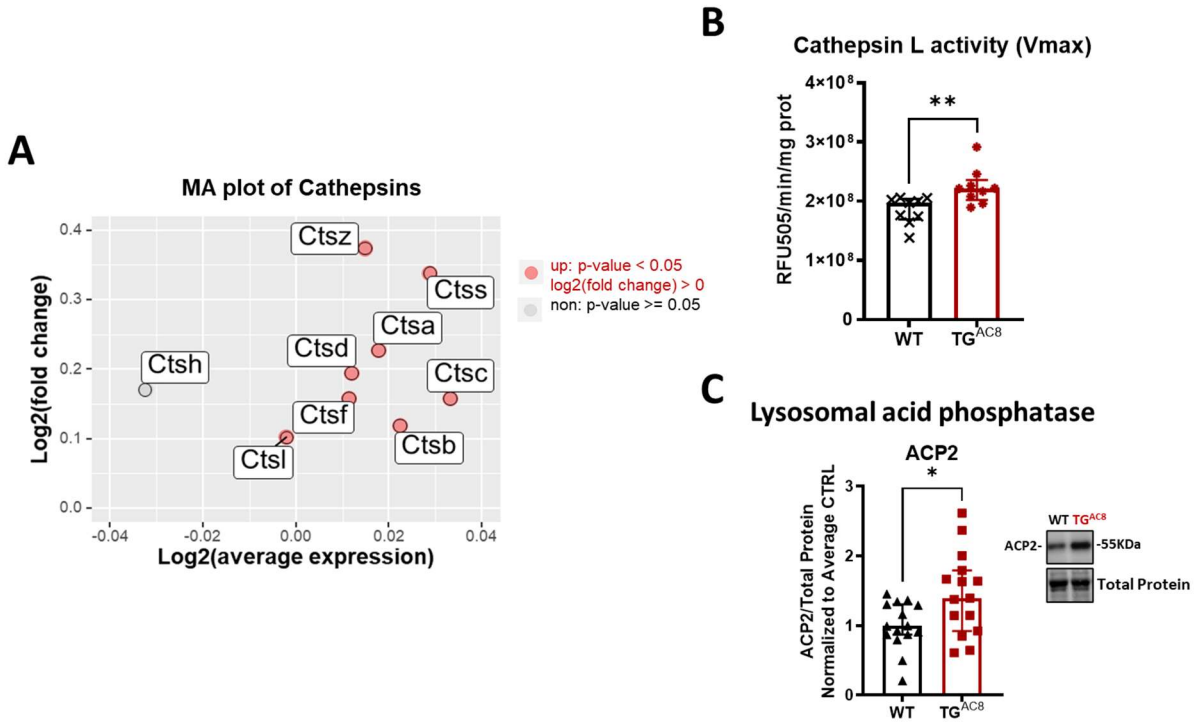

824

825 **Figure 3. Lysosome performance is higher in TG^{AC8} at 3-4 months of age.**

826 **A**), MA plot showing enrichment in the relative amount of lysosomal cathepsin obtained

827 from OMICs data in TG^{AC8} at 3 months of age. **B**), Cathepsin L1 activity measured in

828 TG^{AC8} and WT littermate at 3 months of age (n=6 mice per group). Activity was measured

829 at V_{max}, and it is plotted as emitted fluorescence per mL, per mg of protein. **C**), Bar graphs

830 and Western blot analysis of the lysosomal acid phosphatase, ACP2 (n=15 mice per

831 group). Unpaired 2-tailed Student t test was used in **B** and unpaired 2-tailed Student t test

832 with Welch's correction was used in **C**. Data are presented as the median ± interquartile

833 range. * indicates significant (<0.05) differences between genotypes (WT vs TG^{AC8}).

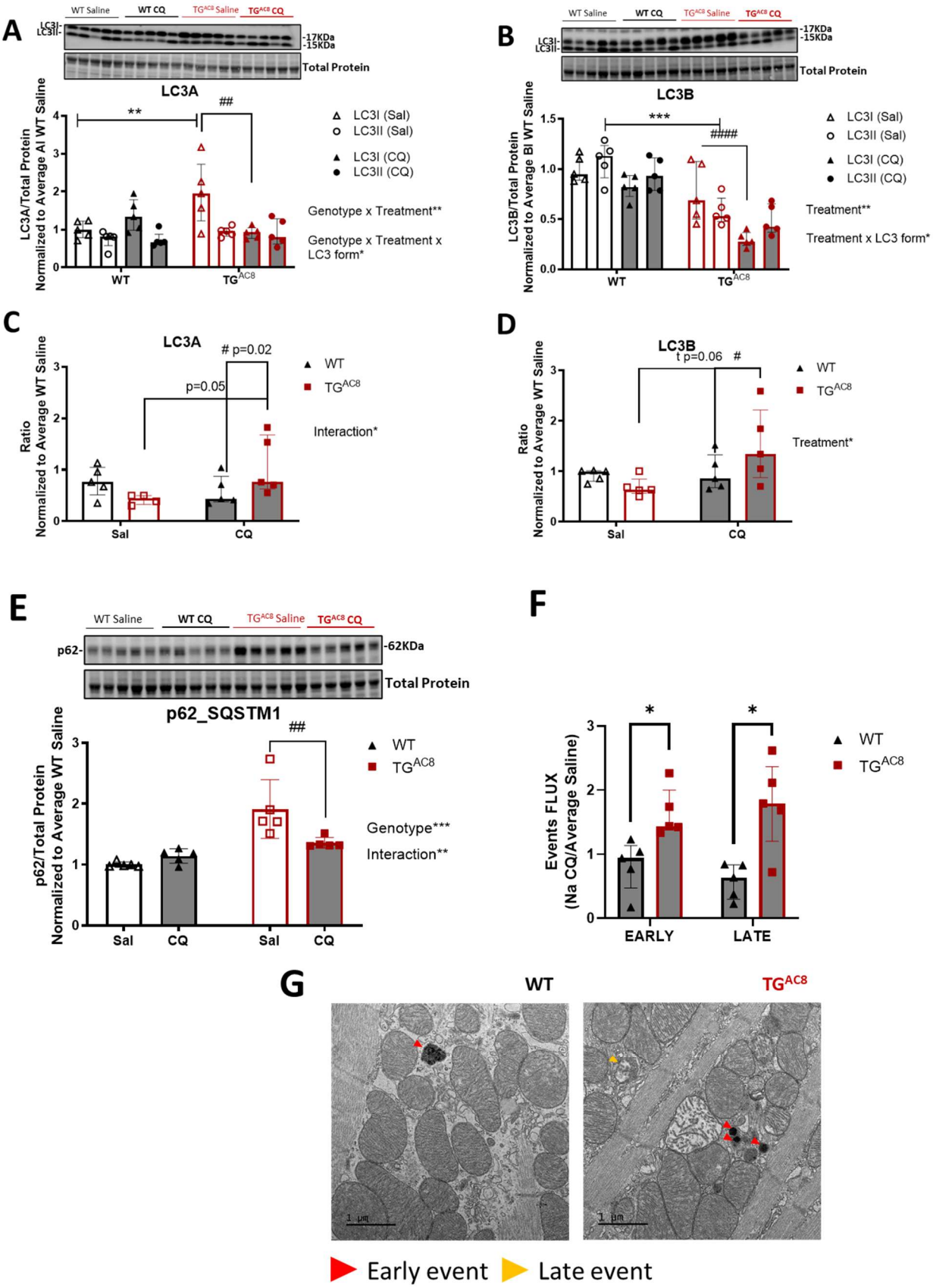
A
WT Saline
WT CQ
TGAC8 Saline
TGAC8 CQ
LC3I-
LC3II-
-17KDa
-15KDa
Total Protein
LC3A
LC3A/Total Protein
Normalized to Average AI WT Saline
**
##
LC3I (Sal)
LC3II (Sal)
LC3I (CQ)
LC3II (CQ)
Genotype x Treatment**
Genotype x Treatment x LC3 form*
WT
TGAC8
B
LC3B
LC3B/Total Protein
Normalized to Average BI WT Saline
***
####
Treatment**
Treatment x LC3 form*
C
LC3A
Ratio
Normalized to Average WT Saline
# p=0.02
p=0.05
Interaction*
Sal
CQ
D
LC3B
t p=0.06 #
Treatment*
E
p62-
-62KDa
p62_SQSTM1
p62/Total Protein
Normalized to Average WT Saline
##
Genotype***
Interaction**
F
Events FLUX
(Na CQ/Average Saline)
*
EARLY
LATE
G
WT
TGAC8
1 µm
Early event
Late event

836 **Figure 4. Autophagic flux is accelerated in TG^{AC8} at 3-4 months of age.**

837 TG^{AC8} and WT at 3-4 months of age were treated by intraperitoneal administration of
838 chloroquine (CQ) (50 mg/kg) or saline, and LVs were collected 3 hours after drug
839 administration and snap-frozen for analysis of autophagy markers LC3, LC3II/LC3I ratios,
840 and p62 (n=5 mice per group). Bar graphs and Western blot analysis of **A**), LC3A; **B**),
841 LC3B; **C**), LC3AII/LC3AI; **D**), LC3BII/LC3BI; **E**), p62; **F**), paired TEM event flux
842 quantification of early and late autophagic figures, normalized to average WT saline; **G**)
843 representative micrographs. **A and B**, A three-way ANOVA with repeated measurements,
844 followed by Original FDR method of Benjamini and Hochberg post-hoc multi-comparison
845 test was used. **C, D, E and F**, A two-way ANOVA, followed by Original FDR method of
846 Benjamini and Hochberg post-hoc multi-comparison test was used. Data are presented
847 as the median ± interquartile range. Symbols indicate significant (<0.05) differences
848 between genotypes* (WT vs TG^{AC8}), between treatments# (CQ vs saline).

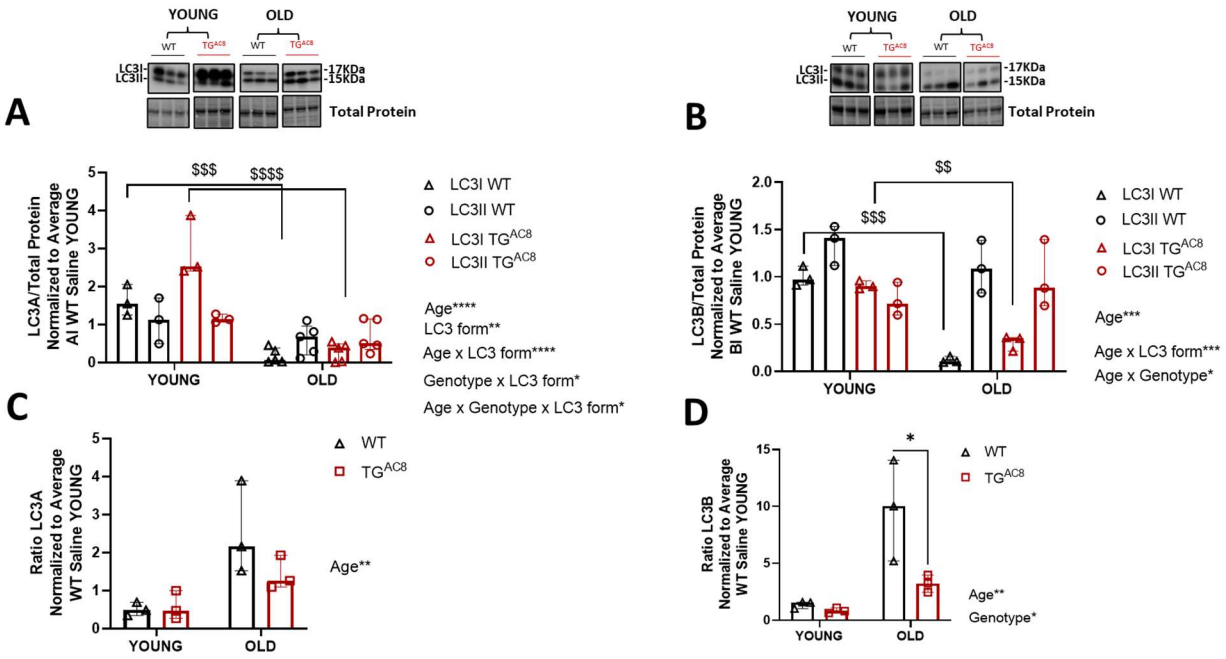
A
YOUNG
OLD
WT
TGAC8
LC3I-
LC3II-
-17KDa
-15KDa
Total Protein
LC3A/Total Protein Normalized to Average AI WT Saline YOUNG
$$$
$$$$
LC3I WT
LC3II WT
LC3I TGAC8
LC3II TGAC8
Age****
LC3 form**
Age x LC3 form****
Genotype x LC3 form*
Age x Genotype x LC3 form*
B
LC3B/Total Protein Normalized to Average BI WT Saline YOUNG
$$
$$$
Age***
Age x LC3 form***
Age x Genotype*
C
Ratio LC3A Normalized to Average WT Saline YOUNG
WT
TGAC8
Age**
D
Ratio LC3B Normalized to Average WT Saline YOUNG
*
Age**
Genotype*

849

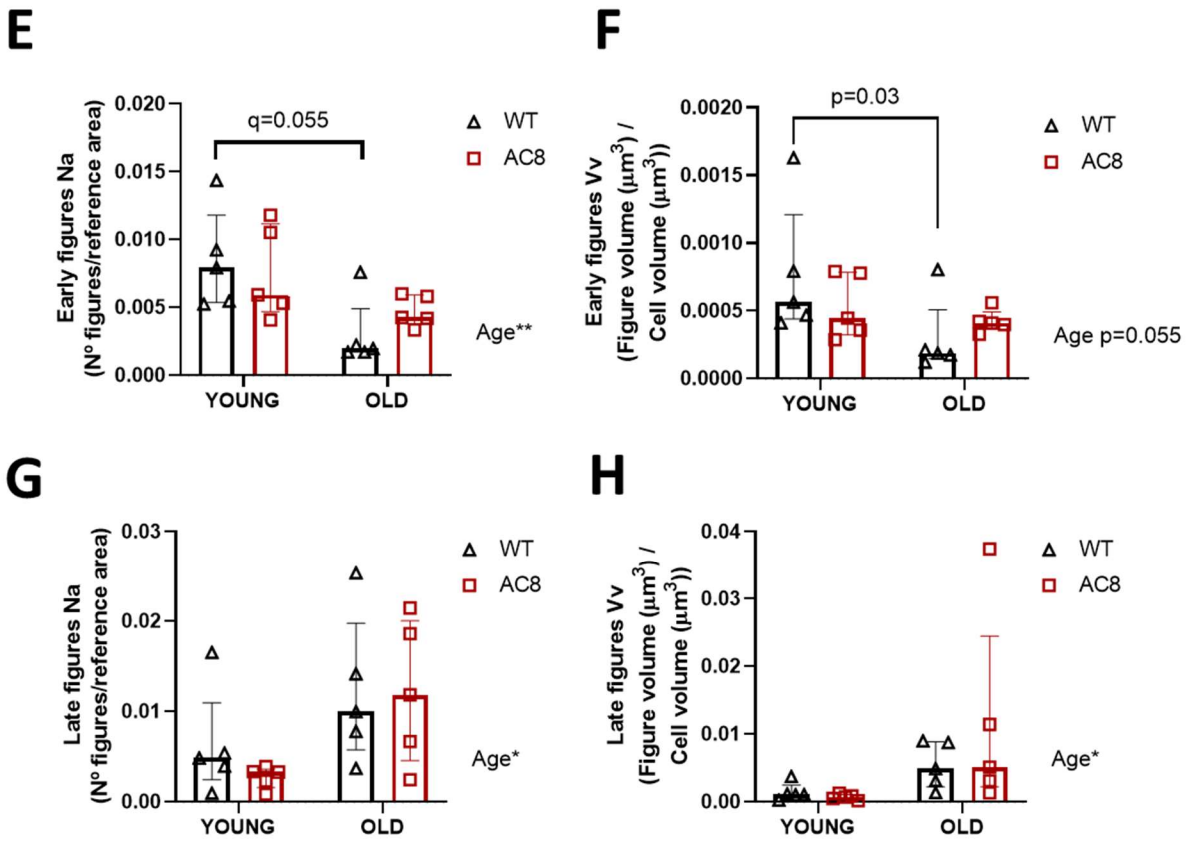
E
Early figures Na (Nº figures/reference area)
q=0.055
WT
AC8
Age**
F
Early figures Vv (Figure volume (µm3) / Cell volume (µm3))
p=0.03
Age p=0.055
G
Late figures Na (Nº figures/reference area)
Age*
H
Late figures Vv (Figure volume (µm3) / Cell volume (µm3))
Age*
YOUNG
OLD

850

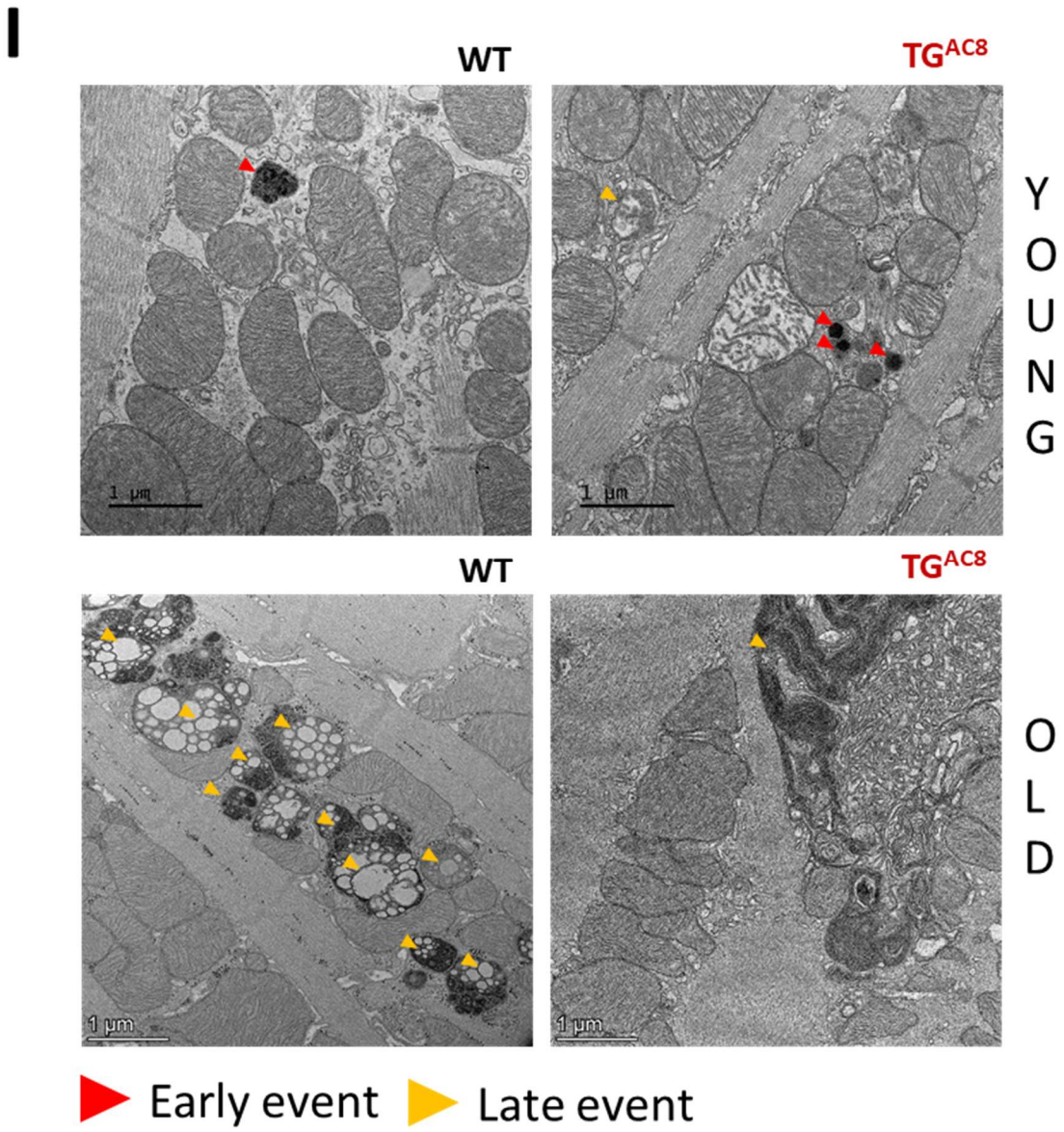

851

852 **Figure 5. Autophagy decline with aging is independent of genotype.**

853 Bar graphs and Western blot analysis of autophagy markers LC3, LC3II/LC3I ratios and
854 p62 in TG^{AC8} and WT at 3-month (n=3 mice per group) and 21-month of age (n=5 mice
855 per group). **A**), LC3A; **B**), LC3B; **C**), LC3AII/LC3AI ratio; **D**) LC3BII/LC3BI ratio. Bar
856 graphs showing the quantification by TEM of autophagic figures (n=5 mice per group) for
857 *early* events **E**), number of per reference area; **F**) volume per cell volume, and for *late*

858 events **G**), number of per reference area, **H**) volumes per cell volume. **I**, TEM
859 representative images. **A and B**, A three-way ANOVA with repeated measurements,
860 followed by Original FDR method of Benjamini and Hochberg post-hoc multi-comparison
861 test was used. **C, D, E, F, G and H**, A two-way ANOVA, followed by Original FDR method
862 of Benjamini and Hochberg post-hoc multi-comparison test was used. Data are presented
863 as the median ± range in A and B, and as median ± interquartile range in all others.
864 Symbols indicate significant (<0.05) differences between genotypes* (WT vs TG^{AC8}),
865 between ages$ (young vs old).

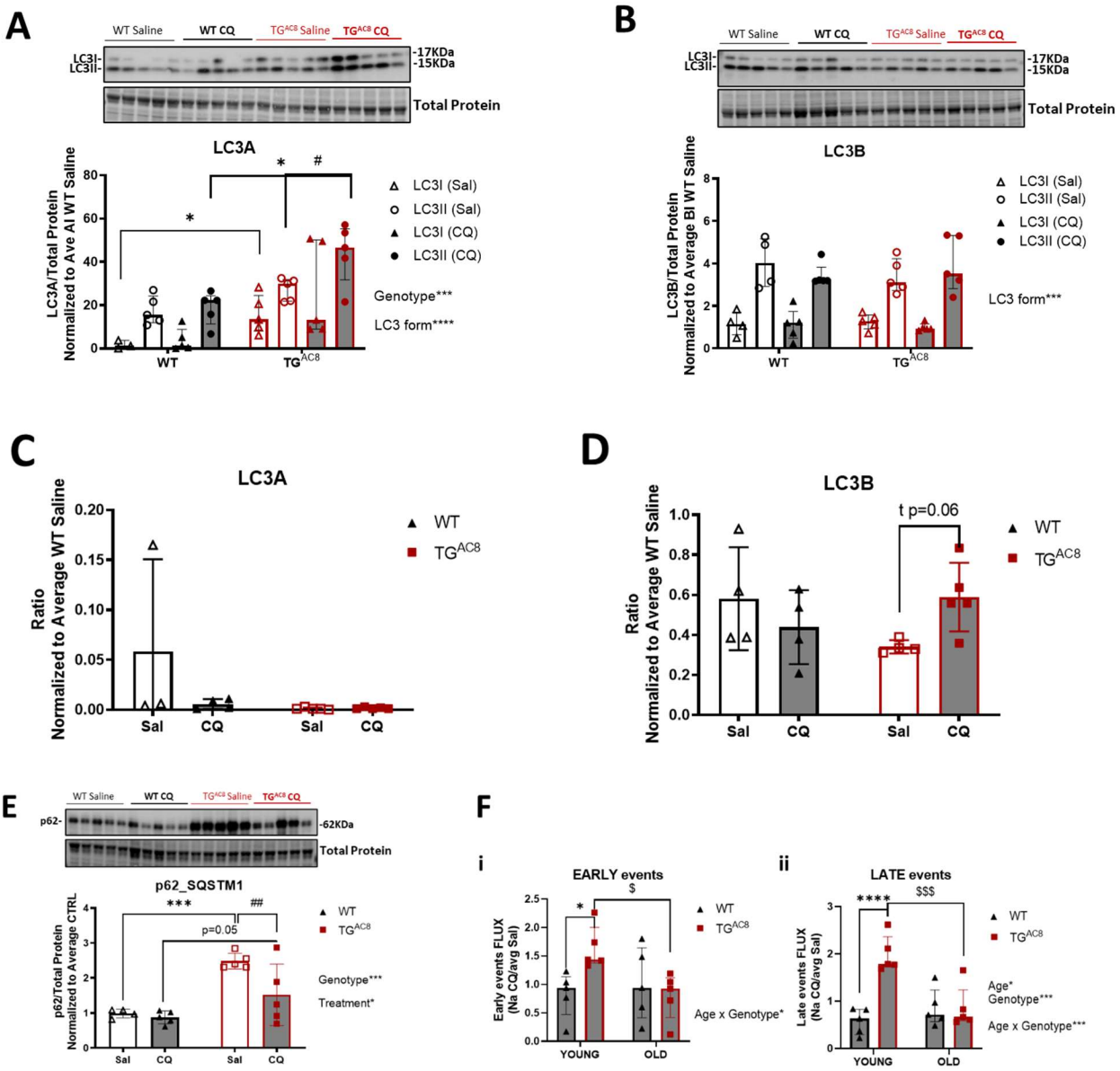

Figure 6. Accelerated autophagic flux in young TG^{AC8} heart becomes maladaptive and insufficient in old age.

TG^{AC8} and WT littermates at 21 months of age were treated by intraperitoneal administration chloroquine (CQ) (50 mg/kg) or saline, and LVs (n=5 mice per group) were collected 3 hours after and snap-frozen for analysis of autophagy markers LC3 and p62. Bar graphs and Western blot analysis of **A**), LC3A; **B**), LC3B; **C**), LC3AII/LC3AI ratio; **D**), LC3BII/LC3BI ratio; **E**), total p62. **F**), paired TEM micrograph quantification of early (**i**)

876 and late (**ii**) autophagic figures, normalized to average WT saline (n=5 mice per group).
877 **A and B**, A three-way ANOVA with repeated measurements, followed by Original FDR
878 method of Benjamini and Hochberg post-hoc multi-comparison test was used. **C, D, E**
879 **and F**, A two-way ANOVA, followed by Original FDR method of Benjamini and Hochberg
880 post-hoc multi-comparison test was used. Data are presented as the median ±
881 interquartile range. Symbols indicate significant (<0.05) differences between genotypes*
882 (WT vs TG^{AC8}), between ages$^{\$}$ (young vs old).

Proteostasis dysregulation is more severe in old TG^{AC8} heart

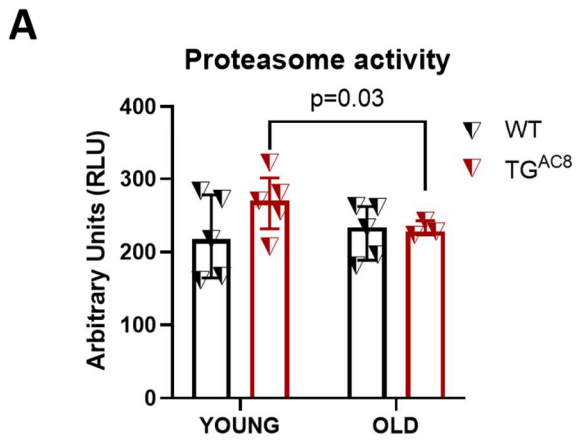

883

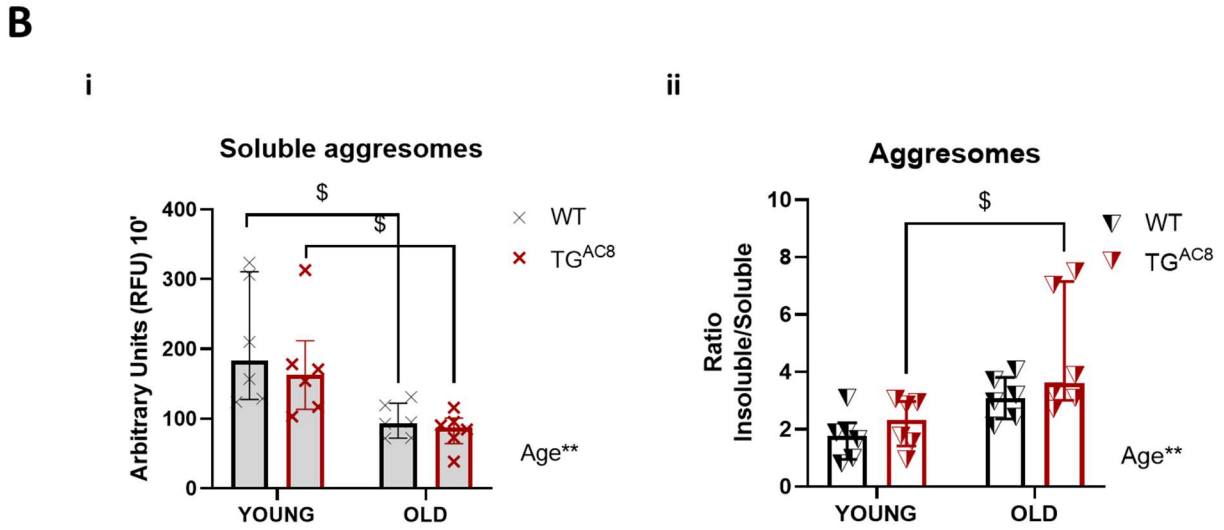

884

885

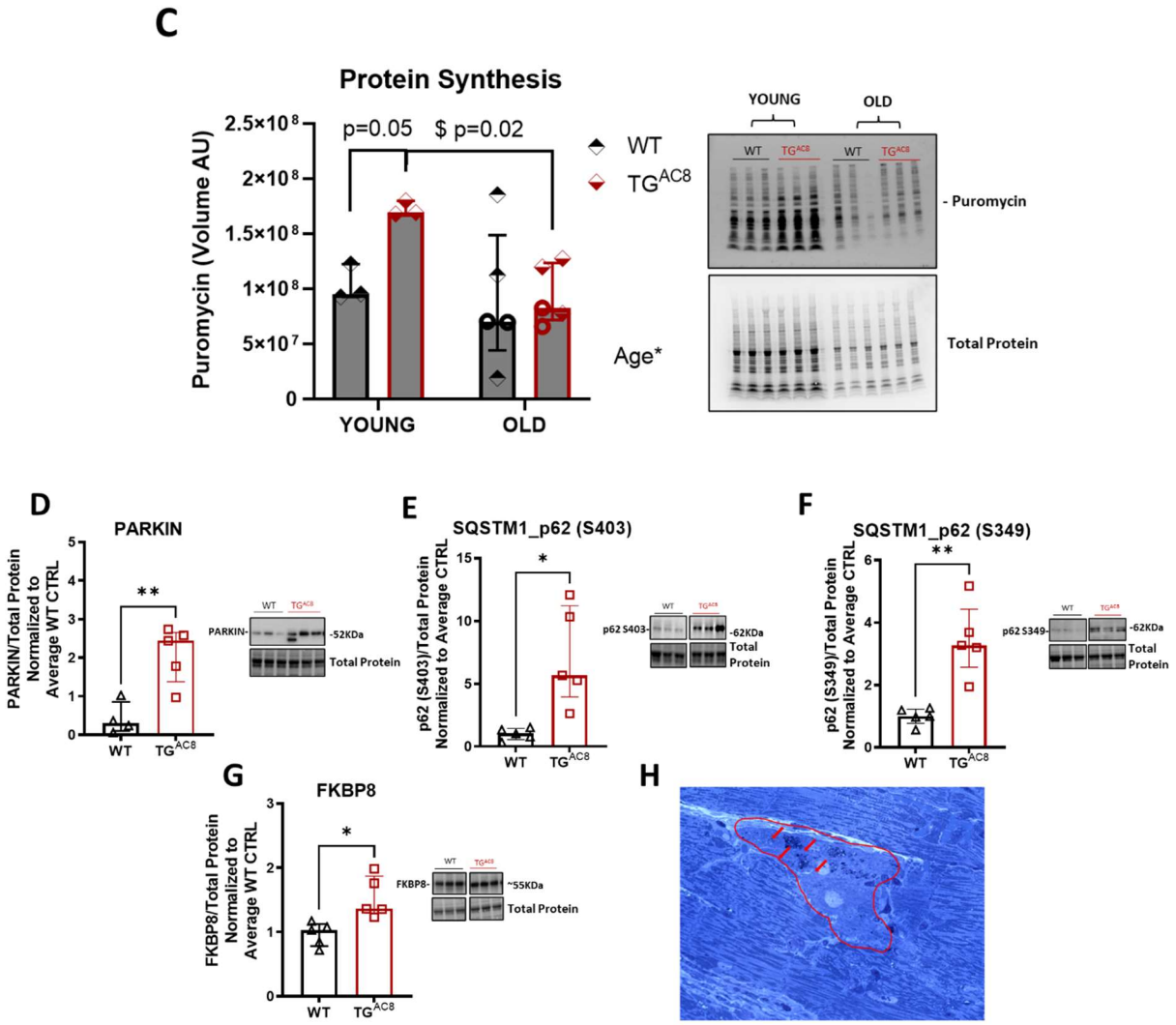

886

887 **Figure 7. Proteostasis dysregulation is more severe in old TG^{AC8} heart.**

888 Bar graphs of **A**), Proteasome activity assessment in old TG^{AC8} (n=3) and WT (n=6) at
889 17-18 months of age) and of **B**), Aggregates quantification in soluble fractions and the
890 ratio of insoluble vs soluble protein aggregates in old TG^{AC8} and WT at 17-18 months of
891 age) (n=5 mice per group). **C**) TG^{AC8} and WT at 19 months of age (n=5 mice per group)
892 were treated by intraperitoneal administration of puromycin (0.022g/g mouse) according
893 to the SUnSET method, and LVs were collected 30 minutes after drug administration and
894 snap-frozen for puromycin analysis. Bar graphs and Western blot analysis of mitophagy

895 canonical cargo receptors (n=5 mice per group, old TG^{AC8} and WT at 21 months of age)
896 **D**), PARKIN; **E**), SQSTM1_p62-S403; **F**), SQSTM1_p62-S349 and the noncanonical
897 cargo receptor **G**) FKBP8. **H**), Semithin staining of old TG^{AC8} LV showing mitochondrial
898 loss of structure. A two-way ANOVA, followed by Original FDR method of Benjamini and
899 Hochberg post-hoc multi-comparison test was used for **Biii, and C**. Unpaired 2-tailed
900 Student t test with Welch's correction was used for **Ai, Aii, Bi, Bii, D**, **E, F and G**. Data
901 are presented as the median ± interquartile range. Symbols indicate significant (<0.05)
902 differences between genotypes* (WT vs TG^{AC8}), between ages$ (young vs old).

Severe proteostasis disruption leads the old TG^{AC8} heart to accelerated aging

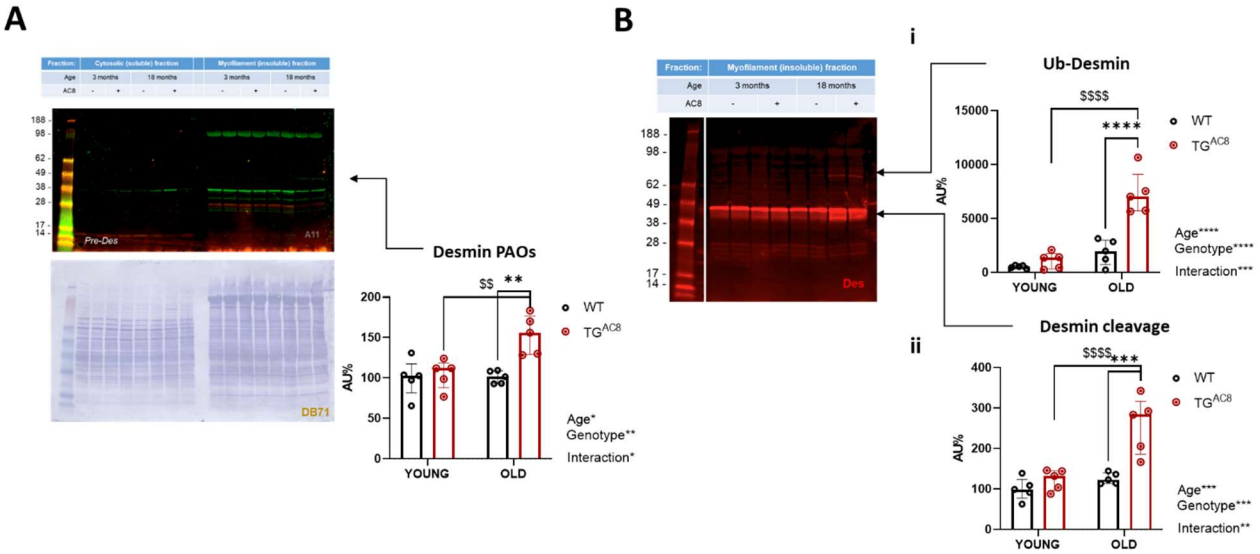

903

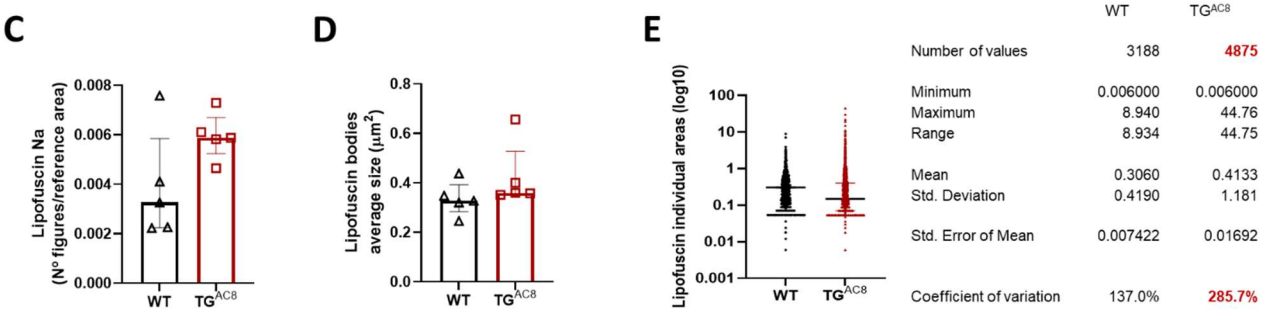

	WT	TG^{AC8}
Number of values	3188	**4875**
Minimum	0.006000	0.006000
Maximum	8.940	44.76
Range	8.934	44.75
Mean	0.3060	0.4133
Std. Deviation	0.4190	1.181
Std. Error of Mean	0.007422	0.01692
Coefficient of variation	137.0%	**285.7%**

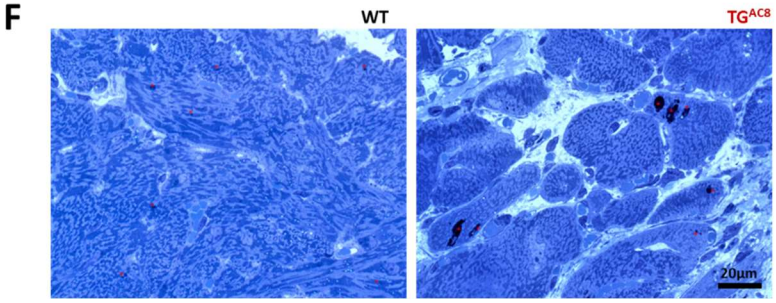

904

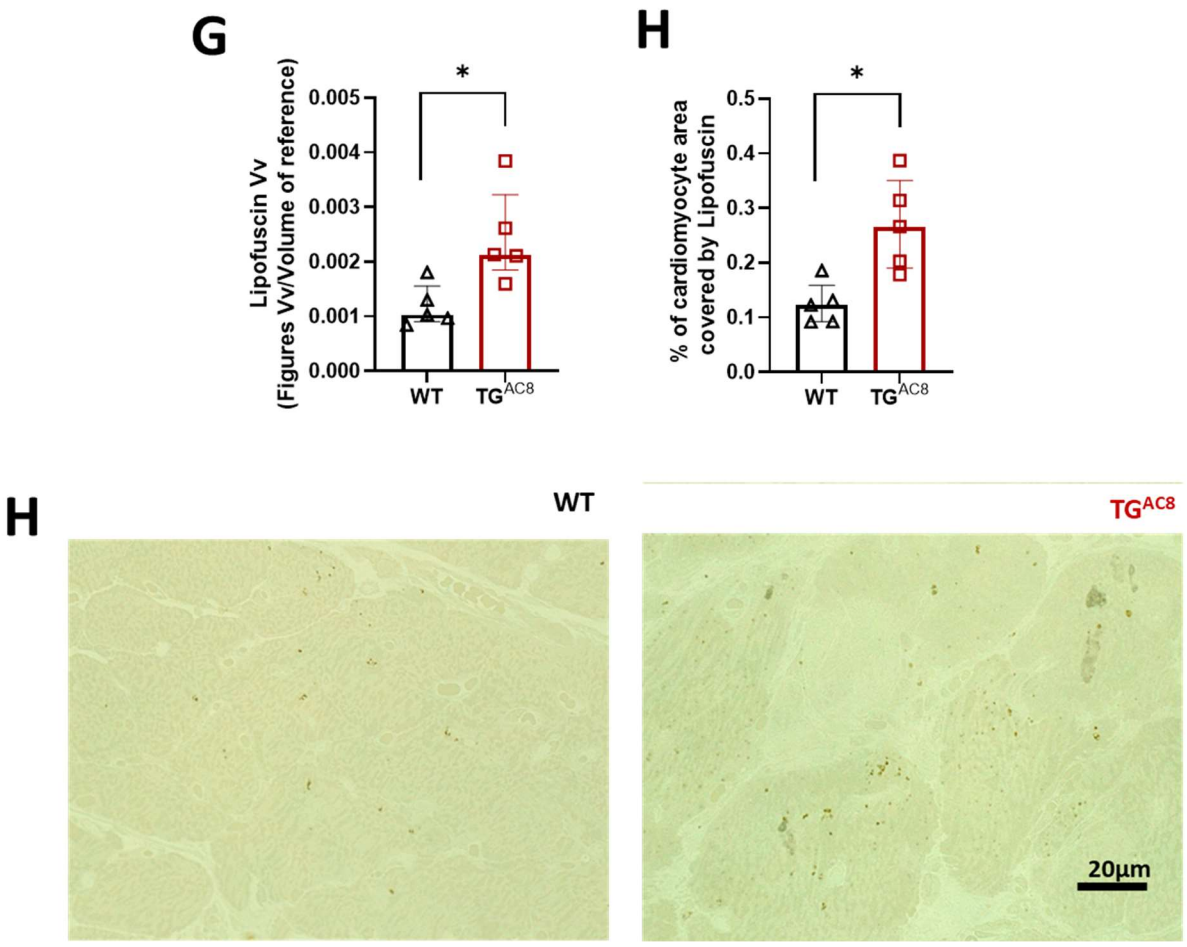

Figure 8. Proteostasis dysregulation by PQC insufficiency leads to increased lipofuscin accumulation and deposition of desmin Pre-Amyloid Oligomers (PAOs) contributing to TG^{AC8} accelerated aging.

Bar graphs representing the quantification of undigested material (LF and desmin) in old TG^{AC8} and WT (n=5 per group); **A**), number of figures per reference area; **B**), average size of lipofuscin bodies; **C**), violin plot showing the more aberrant sizes of lipofuscin bodies; **D**), Representative semi-thin staining of lipofuscin bodies; **E**), volume of figures per volume of reference area; **F**) percentage of cardiomyocyte area covered by lipofuscin; **G**), Representative image of Palade staining of TEM semi-thin sections showing the presence of brown to black pigments in old TG^{AC8} and age-matched WT; **H**), soluble and insoluble (myofilament-enriched) fractions probed with the A11 antibody for pre-amyloid

917 oligomers (top), and total protein staining (Direct Blue71, DB71), with relative
918 densitometry analysis; **I**), insoluble (myofilament-enriched) fractions probed with the
919 desmin antibody, and relative densitometry for **i**) ubiquitinated and **ii**) cleaved desmin
920 proteoforms, in old TG^{AC8} age-matched WT. **A, B**, **C, E**, **and F**, Unpaired 2-tailed Student
921 t test with Welch's correction was used; **L and M**, A two-way ANOVA, followed by Original
922 FDR method of Benjamini and Hochberg post-hoc multi-comparison test was used. Data
923 are presented as the median ± interquartile range. Symbols indicate significant
924 differences (<0.05) between genotypes* (WT vs TG^{AC8}), between ages$ (young vs old).

925 ## SUPPLEMENTAL MATERIAL

926 Table1

Protein Name	Symbol	log2(average expression)	log2(fold change)	p-value
Lysosomal protective protein	Ctsa	0.017702383	0.216799716	0.004513026
Cathepsin B	Ctsb	0.022381593	0.120723106	0.0254094
Dipeptidyl peptidase 1	Ctsc	0.033052876	0.167723218	0.028205766
Cathepsin D	Ctsd	0.011868307	0.164671994	0.033523037
Cathepsin F	Ctsf	0.011385877	0.134158334	0.03797905
Pro-cathepsin H	Ctsh	-0.032543079	0.171483139	0.115212134
Cathepsin L1	Ctsl	-0.002089995	0.082015669	0.037159714
Cathepsin S	Ctss	0.028762851	0.317183952	0.007053072
Cathepsin Z	Ctsz	0.014751699	0.403327276	0.008561447

927

928 **Supplemental Table Relative cathepsin expression in TG^{AC8} at 3 months of age.**
929 ProteOMICs data in TG^{AC8} at 3 months (n=4 mice per group).

930 Figures S1–S5

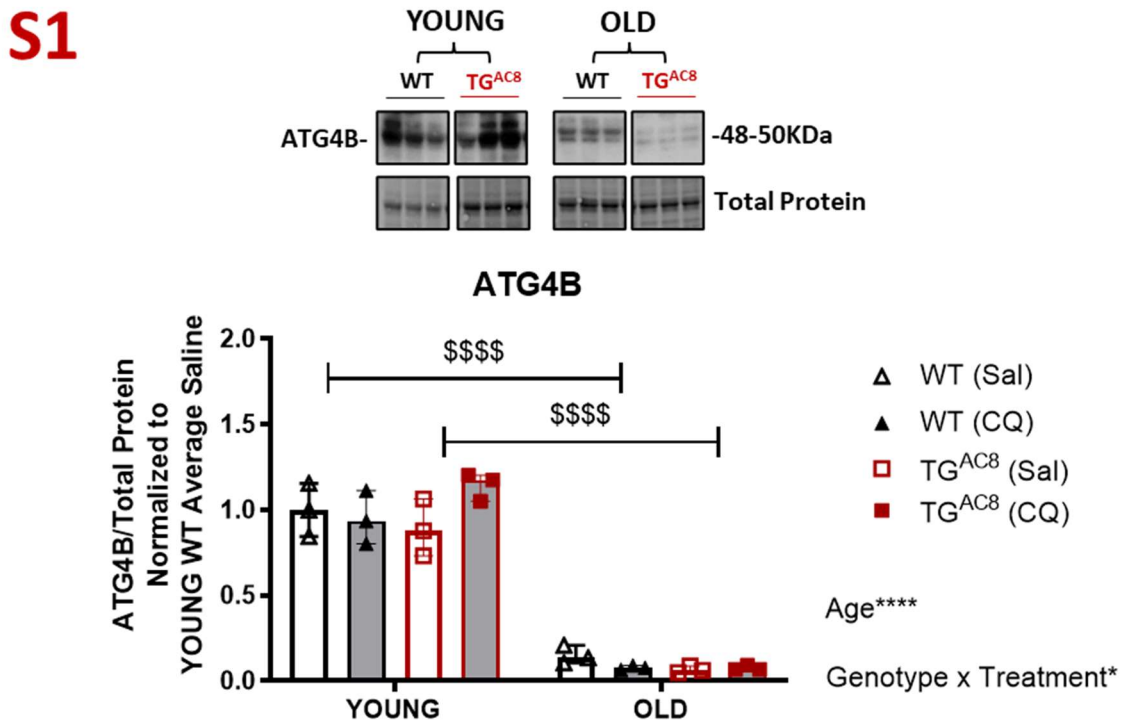

931

932 **Figure S1. ATG4B expression with aging in TG^{AC8} vs WT.**

933 Bar graphs and WB analysis of ATG4B in TG^{AC8} and WT littermates LVs at 3 months and

934 21 months of age (n=3 mice per group). A three-way ANOVA followed by Original FDR

935 method of Benjamini and Hochberg post-hoc multi-comparison test was used. Data are

936 presented as the median ± range.

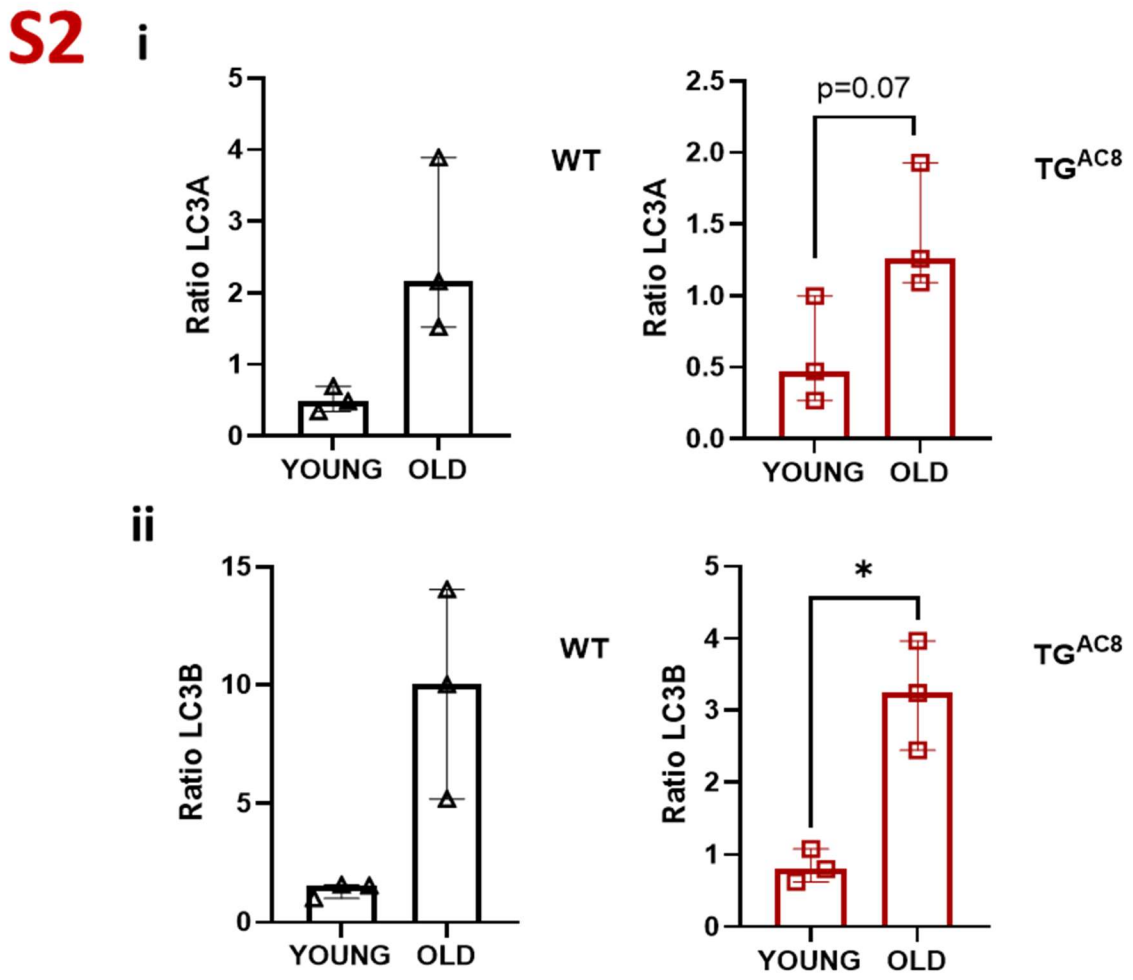

937

938 **Figure S2. LC3II/LC3I ratios increase with aging in TG^{AC8} vs WT.**

939 Bar graphs and Western blot analysis of LC3II/LC3I ratios in young (3 months) and old

940 (21 months) WT and TG^{AC8} LVs (n=3 mice per group). **i**) LC3AII/LC3AI ratio; **ii**),

941 LC3BII/LC3BI ratio. Unpaired 2-tailed Student t test with Welch's correction was used.

942 Data are presented as the median ± interquartile range.

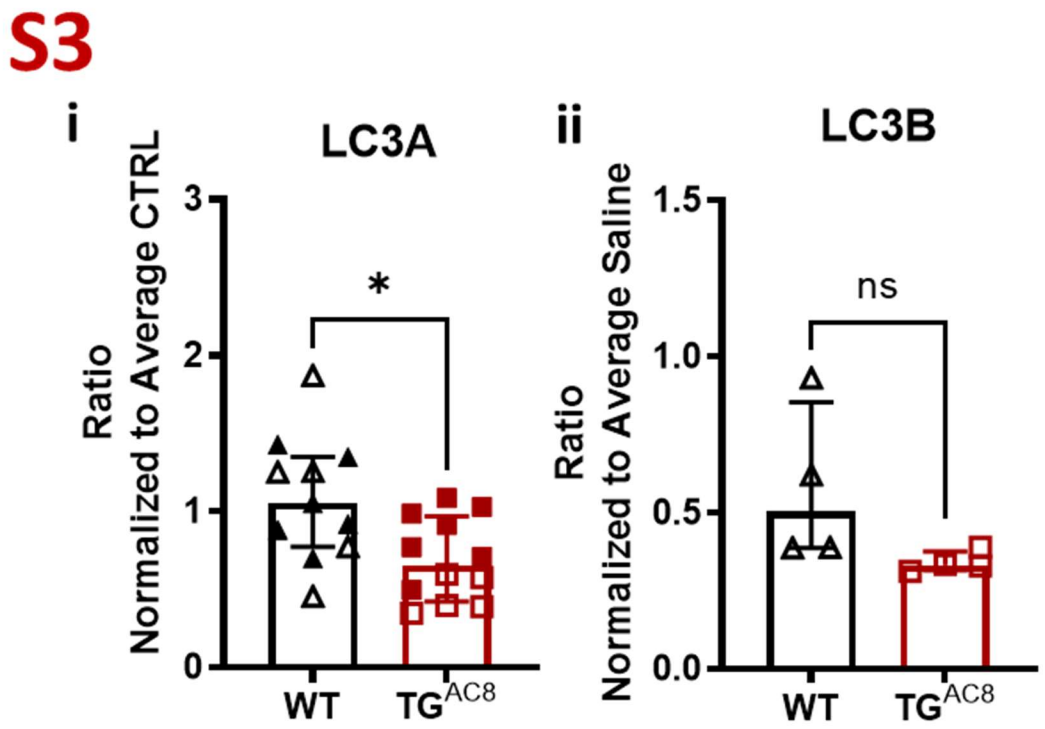

943

944 **Figure S3. LC3II/LC3I ratios is significantly downregulated in old TG^{AC8} vs age-**
945 **matched WT.**

946 Bar graphs and Western blot analysis of LC3II/LC3I ratios in old (21 months) WT and
947 TG^{AC8} LVs. **i**) LC3AII/LC3AI ratio (n=11 mice in the WT group, n=12 mice in the TG^{AC8}
948 group); **ii**) LC3BII/LC3BI ratio (n=5 mice per group). Unpaired 2-tailed Student t test with
949 Welch's correction was used. Data are presented as the median ± interquartile range.

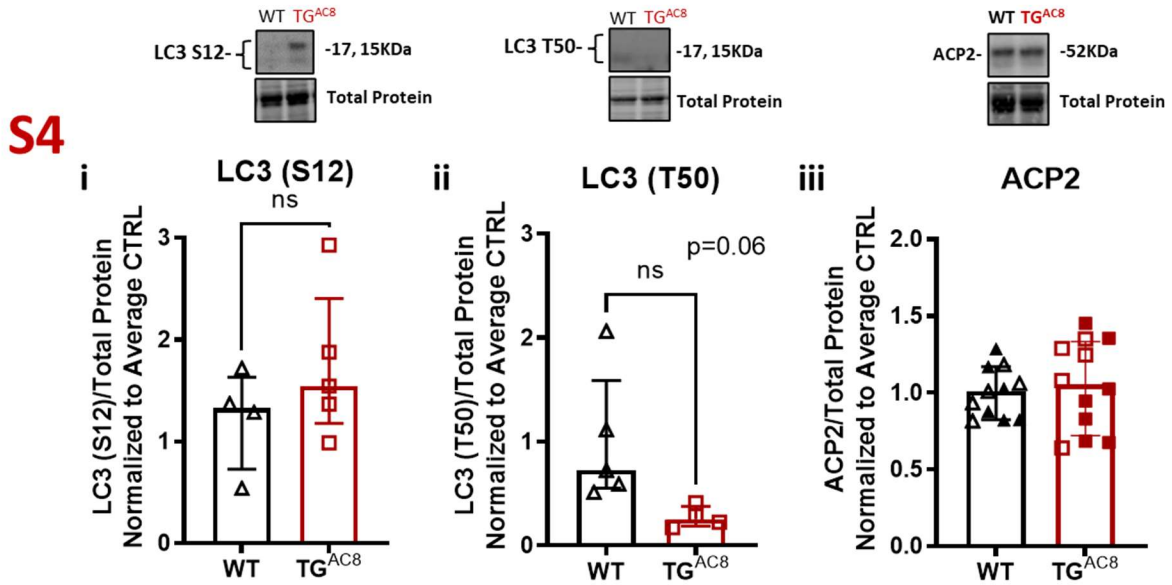

Figure S4. Autophagy marker expression in old TG^{AC8} vs age-matched WT. Bar graphs and Western blot analysis of LC3 phospho-forms and the lysosomal hydrolase ACP2 in old TG^{AC8} and WT LVs at 21 months of age. **i**), LC3-S12 and **ii**) LC3-T50 (n=5 mice per group); **iii**), ACP2 (n=11 mice WT group, n=12 mice TG^{AC8} group. Unpaired 2-tailed Student t test with Welch's correction was used in **A and B**. Unpaired 2-tailed Student t test was used in **C**. Data are presented as the median ± interquartile range.

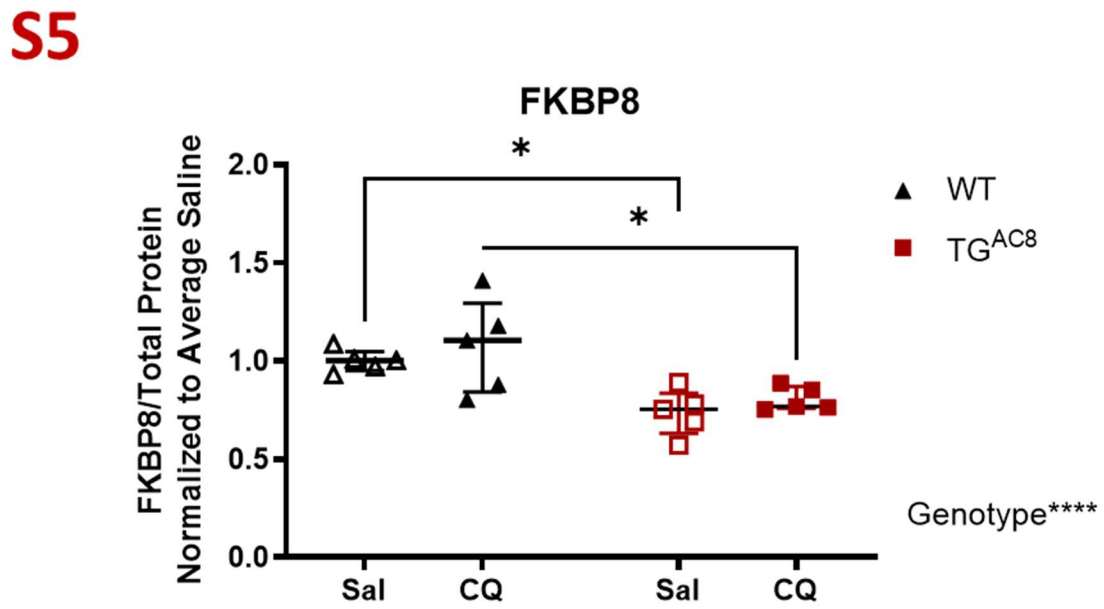

957

958 **Figure S5. Non-canonical mitophagy receptor FKBP8 levels are decreased in TG^{AC8}**
959 **vs WT at 3-4 months of age.**

960 TG^{AC8} and WT littermates at 3 months of age were treated by intraperitoneal
961 administration chloroquine (CQ) (50 mg/kg) or saline, and LVs (n=5 mice per group) were
962 collected 3 hours after and snap-frozen for analysis of the non-canonical mitophagy
963 receptor FKBP8 A two-way ANOVA, followed by Original FDR method of Benjamini and
964 Hochberg post-hoc multi-comparison test was used. Data are presented as the median ±
965 interquartile range.